

# Chapter 2

## Electronic Phase Separation and Glassy Behavior in Magnetic Perovskites

### 2.1 Introduction

Complex transition metal-based  $\text{ABO}_3$  perovskites are known to exhibit compositional and electronic inhomogeneities arising from the existence of more than one phase in crystals of nominally monophasic composition, with the different phases in such materials having comparable compositions [1, 2]. Magnetic perovskites display a variety of effects due to such phase separation giving rise to novel electronic and magnetic properties. In the perovskite family the manganites became popular because of the colossal magnetoresistance (CMR) exhibited by them as discussed earlier in Section A [1–9]. CMR and related properties are generally explained on the basis of the double-exchange (DE) mechanism of the electron hopping between the  $\text{Mn}^{3+}(\text{t}_{2g}^3\text{e}_g^1)$  and  $\text{Mn}^{4+}(\text{t}_{2g}^3\text{e}_g^0)$  ions. Jahn–Teller (J–T) distortion associated with the  $\text{Mn}^{3+}$  ions and charge ordering (CO) of the  $\text{Mn}^{3+}$  and  $\text{Mn}^{4+}$  ions compete with DE and favor insulating behavior and antiferromagnetism [1]. CO in these materials is closely linked to the ordering of the orbitals. Typical of charge-ordered manganites are  $\text{Pr}_{1-x}\text{Ca}_x\text{MnO}_3$  ( $x = 0.3\text{--}0.4$ ) and  $\text{Nd}_{0.5}\text{Ca}_{0.5}\text{MnO}_3$  which show CO around 250 K and antiferromagnetic ordering (A-type) at lower temperatures [4]. The CO states can be melted into metallic state by applying high magnetic fields. On the other hand,  $\text{Nd}_{0.5}\text{Sr}_{0.5}\text{MnO}_3$  is ferromagnetic below room temperature and shows CO at lower temperatures ( $\sim 150$  K) accompanied by antiferromagnetism (CE-type). The nature of phase separation in the perovskite manganites depends on the average size of the A-site cations and the associated size disorder, carrier concentration or the composition (value of  $x$ ), temperature, and other external factors such as magnetic and electric fields. Phases with different charge densities (carrier concentrations) as well as magnetic and electron transport properties coexist as carrier-rich ferromagnetic (FM) clusters or domains along with a carrier-poor antiferromagnetic (AFM) phase. Such an electronic phase separation giving rise to microscopic or mesoscopic inhomogeneous distribution of electrons results in a rich phase diagram [2]. What is noteworthy is that electronic phase separation is likely

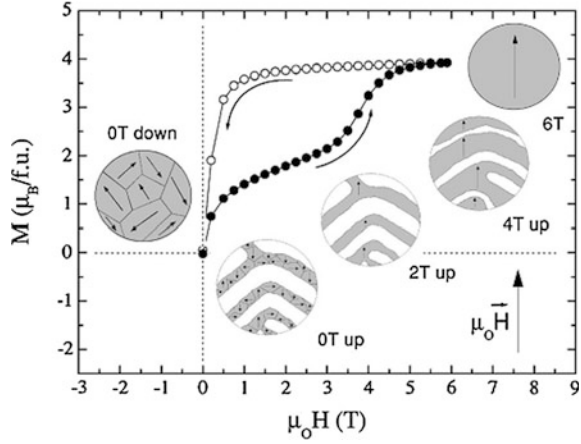
to be a general property of solids with correlated electrons such as the large family of transition metal oxides. There are indications that many of the unusual magnetic and electron transport properties of magnetic perovskites arise from phase separation.

The term phase separation or segregation implies the presence of at least two distinct phases in the sample, but the relative fractions may vary anywhere from a dilute regime, involving small domains of the minor phase (or clusters) in the matrix of the major phase, to a situation in which the fractions of the two phases are comparable. Thus, FM clusters present randomly in an AFM host matrix often give rise to a glassy behavior. As the FM clusters in an AFM matrix grow in size to become reasonably sized domains, due to effect of temperature, composition, or an applied magnetic field, the system acquires the characteristics of a genuine phase-separated system. In this section, we discuss electronic phase separation and associated effects in magnetic and electron transport properties in disordered perovskite manganites and cobaltites. The latter system also exhibits ferromagnetism and metallicity when the average size of the cations is sufficiently large and the size disorder is not excessive. The ferromagnetism in the perovskite cobaltites is considered to be due to  $\text{Co}^{3+}\text{--O--Co}^{4+}$  superexchange interactions.

## 2.2 Manganese-Centered Magnetic Perovskites

The first report on electronic phase separation (EPS) in perovskite manganites  $\text{La}_{1-x}\text{Ca}_x\text{MnO}_3$  was presented by Wollen and Koehler [1]. They observed the presence of both FM and AFM peaks in the magnetic structure of  $\text{La}_{1-x}\text{Ca}_x\text{MnO}_3$  by neutron scattering, and hence drew the conclusion that there is the simultaneous presence of FM and AFM phases in this material in 1950s [1]. In order to understand the magnetic and electron transport properties, CMR effect, etc. of magnetic perovskites, EPS is getting accepted as the phenomenon of importance [2–9]. However, for the nanoscopic electronic inhomogeneity in magnetic perovskites, both TEM, high-resolution TEM and scanning transmission electron microscopy (STEM) and STM can be used to find out the coexistence of nanoscopic charge-ordered (insulating) domains and the FM metallic domains, giving the local structural information at atomic level [9]. Due to the sensitivity of phase separation to magnetic fields, it is often difficult to identify EPS based on the magnetization and transport measurements. Teresa et al. [4] have reported on the experimental evidence for the existence of nanoscopic EPS in the perovskites of  $(\text{La}_{1-x}\text{A}_x)_{2/3}\text{Ca}_{1/3}\text{MnO}_3$  ( $\text{A} = \text{Y}$  or  $\text{Tb}$ ). In their report it was revealed that by a combination of volume thermal expansion, magnetic susceptibility, and small-angle neutron scattering measurements, there is a spontaneous formation of localized magnetic clusters with size of  $\sim 1\text{--}2$  nm above the ferromagnetic ordering temperature. Similarly, using small-angle magnetic neutron scattering, Mercone et al. [4] have correlated the evolution of FM phases induced by the magnetic field in a crystal of  $\text{Pr}_{0.67}\text{Ca}_{0.33}\text{MnO}_3$  (Fig. 2.1). The modern technologies such as scanning

**Fig. 2.1** Isotherm magnetization of  $\text{Pr}_{0.67}\text{Ca}_{0.33}\text{MnO}_3$  at 30 K as a function of magnetic field and the schematic representation of EPS (adapted from Mercone et al. [4])



electron nanodiffraction, atomic-resolution STM, MFM, and electron holography have been developed that directly identify the EPS phenomenon in low-dimensional perovskite manganite nanostructures [2, 4, 6, 7]. Along with the development of nanotechnology, the EPS phenomenon in perovskite-based CMR nanoparticles has also received great attention. In recent years, the evolution of the EPS with magnetic field in perovskite nanoparticles has been reported by several groups, which has a significant impact on the perovskite-based nanoelectronics [7].

Meanwhile, Fäth et al. [7] also discovered the evidence for electronic inhomogeneities in  $\text{La}_{0.7}\text{Ca}_{0.3}\text{MnO}_3$  by STM, below the FM transition temperature with a mesoscopic scale of about  $0.2 \mu\text{m}$  where the FM metallic domains are interspersed in insulating regions. EPS involving submicrometer-sized FM and charge-ordered AFM domains with a typical size of about  $0.2 \mu\text{m}$  was demonstrated in  $\text{La}_{0.625-y}\text{Pr}_y\text{Ca}_{0.375}\text{MnO}_3$  by TEM study [9]. Mesoscopic phase separation arising from the comparable energies of the ferromagnetic metallic and antiferromagnetic insulating states, with the length scale between 30 and 200 nm, is just one extreme in the perovskite manganites [9]. The EPS with phases of different charge densities is usually expected to give rise to nanometer-scale clusters as large phase-separated domains would break up into small pieces due to the Coulomb interactions. In general, microscopically homogenous clusters often ranging in their diameter size of 1–2 nm are dispersed in an insulating or charge-localized matrix. One can visualize EPS arising from disorder as well, which could arise from the size mismatch of the A-site cations in the perovskite structure [3]. Such EPS is seen in the  $(\text{La}_{1-y}\text{Pr}_y)_{1-x}\text{Ca}_x\text{MnO}_3$  system in terms of a metal–insulator transition induced by disorder [9]. The size of the clusters depends on the magnitude of disorder. The smaller the disorder, the large would be the size of the clusters. This could be the reason why high magnetoresistance occurs in perovskites with small disorder.

Microscopically homogeneous clusters are usually of the size of 1–2 nm in diameter dispersed in an insulating or charge-localized matrix. Such an EPS scenario bridges the gap between the DE model and the lattice distortion models.

Several publications on the perovskite manganites reveal that in addition to microscopic phase separation, there can be mesoscopic phase separation where the length scale is between 1 and 200 nm, arising from the comparable energies of the FM metallic and AFM insulating states [1, 2, 5, 9-11].

### 2.2.1 Electronic Phase Separation (EPS) in $(La_{1-x}Ln_x)_{0.7}Ca_{0.3}MnO_3$ ( $Ln = Pr, Nd, Gd, \text{ and } Y$ )

In  $(La_{1-y}Pr_y)_{1-x}Ca_xMnO_3$  perovskites, submicrometer-sized EPS involving FM and charge-ordered AFM domains has been observed. By varying composition, the volume fraction and the domain size of the FM and charge-ordered phases could be varied [9-11]. The corresponding magnetization and resistivity data for  $La_{0.5-x}Ln_xCa_{0.5}MnO_3$  ( $Ln = Pr, Nd$ ) is presented in Fig. 2.2. These properties comprehensively describe the competing interactions between FM and CO/OO states and the resultant phase separation are most prominently observed.

We presented in Fig. 2.3, the temperature-dependent magnetic properties of  $(La_{1-x}Nd_x)_{0.7}Ca_{0.3}MnO_3$  perovskites, which represents the sensitivity magnetic

**Fig. 2.2** Temperature variation of the  
**a** magnetization,  $M$ , and  
**b** resistivity,  $\rho$ ,  
of  $La_{0.5-x}Ln_xCa_{0.5}MnO_3$   
( $Ln = Pr, Nd$ ) (adapted from  
Ref. [10]; Kundu et al.)

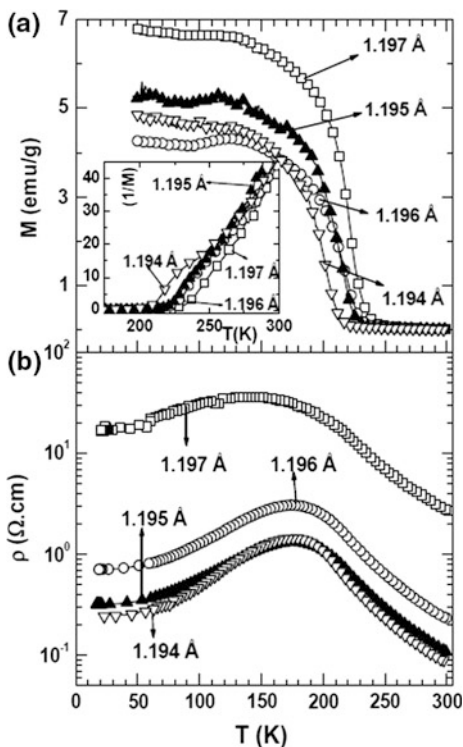
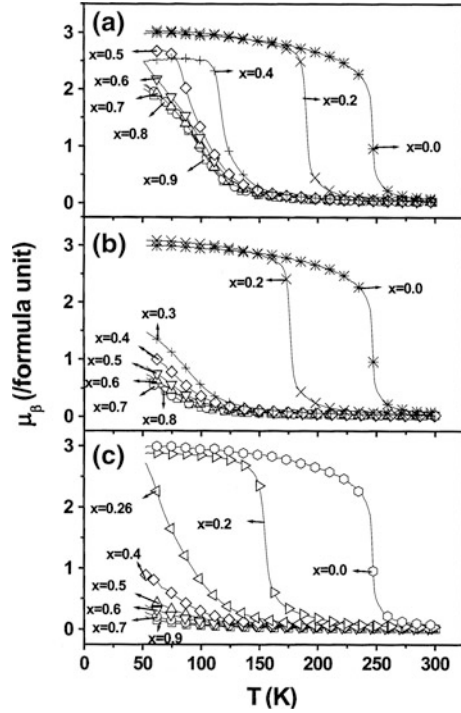


**Fig. 2.3** Temperature variation of magnetic moment ( $\mu_B$ ) in the manganites.

**a**  $(\text{La}_{1-x}\text{Nd}_x)_{0.7}\text{Ca}_{0.3}\text{MnO}_3$ ,  
**b**  $(\text{La}_{1-x}\text{Gd}_x)_{0.7}\text{Ca}_{0.3}\text{MnO}_3$ ,  
 and **c**  $(\text{La}_{1-x}\text{Y}_x)_{0.7}\text{Ca}_{0.3}\text{MnO}_3$   
 (adapted from Sudheendra et al. [10])



moment ( $\mu_B$ ) to the substitution of La by the smaller cation Nd. The FM  $T_C$  shifts to lower temperature with increase in  $x$ , a clear FM behavior is observed up to  $x = 0.5$  with a saturation magnetic moment close to 3  $\mu_B$ .

Beyond  $x \geq 0.6$ , there is no magnetic saturation and the highest value of magnetic moment is less than 3  $\mu_B$ . The perovskite composition up to which clear FM behavior appears is defined as the critical composition  $x_c$  [10]. Whereas, the compositions with  $x > x_c$  show a gradual increase in the magnetization at low temperature. In Gd-substituted perovskites, FM  $T_C$  is observed only for the doping concentration of  $0.0 \leq x \leq 0.3$ . The  $x_c$  ( $\sim 0.3$ ) value for Gd-substituted perovskites is much lower than the Nd perovskites ( $\sim 0.6$ ). These features show that  $x_c$  decreases with the average radius of the A-site cation,  $\langle r_A \rangle$  (Fig. 2.3b), which are similar to the reported manganite perovskites by Terashita and Neumeier [12]. Similarly, Y-substituted perovskites exhibit ferromagnetism only for  $x \leq 0.2$  and the FM  $T_C$  decreases with increase in  $x$  value (Fig. 2.3c). Hence for the series of  $(\text{La}_{1-x}\text{Ln}_x)_{0.7}\text{Ca}_{0.3}\text{MnO}_3$  perovskite, the  $x_c$  values are 0.75, 0.6, 0.3, and 0.2 for  $\text{Ln} = \text{Pr}$ ,  $\text{Nd}$ ,  $\text{Gd}$ , and  $\text{Y}$ , respectively, representing a crucial dependence of  $x_c$  on  $\langle r_A \rangle$ . Furthermore, for these magnetic perovskites the FM is replaced with CO/OO with increase in  $x$ , which could be interpreted in terms of the change in electronic bandwidth ( $W$ ). Also, the major change in the magnetization around  $x_c$  in these magnetic perovskites with constant carrier concentration could be attributed to electronic phase separation due to size disorder caused by substitution of the

smaller rare earth cations in place of La. In the Pr-substituted perovskite, the EPS has been reported in the regime of  $x \sim x_c$  ( $x \sim 0.6\text{--}0.8$ ) [11]. These results also support the explanation provided by De Teresa et al. [13], where they have reported FMM behavior for low  $x$  and spin glass behavior for large  $x$  ( $\geq 0.33$ ) in perovskite  $(\text{La}_{1-x}\text{Tb}_x)_{0.67}\text{Ca}_{0.33}\text{MnO}_3$ .

Temperature variation resistivity behavior of  $(\text{La}_{1-x}\text{Ln}_x)_{0.7}\text{Ca}_{0.3}\text{MnO}_3$  (Ln = Nd, Gd, and Y) series of perovskites exhibit somewhat resemblance to the magnetic transition, the  $x \leq x_c$  compositions show insulator–metal (I–M) transition near the FM  $T_C$  (Fig. 2.4). For  $x > x_c$  the perovskites are insulating and do not exhibit any resistivity transition. The I–M transition,  $T_{\text{IM}}$ , for  $x \leq x_c$  compositions decreases linearly with increase in doping concentration (Fig. 2.5). The  $T_{\text{IM}}$  versus  $\langle r_A \rangle$  plot is linear with a positive slope as expected (inset of Fig. 2.5) and no resistivity anomaly at  $T$  ( $< T_{\text{IM}}$ ) for any of these compositions unlike reported by Uehara et al. [9] and Deac et al. [14].

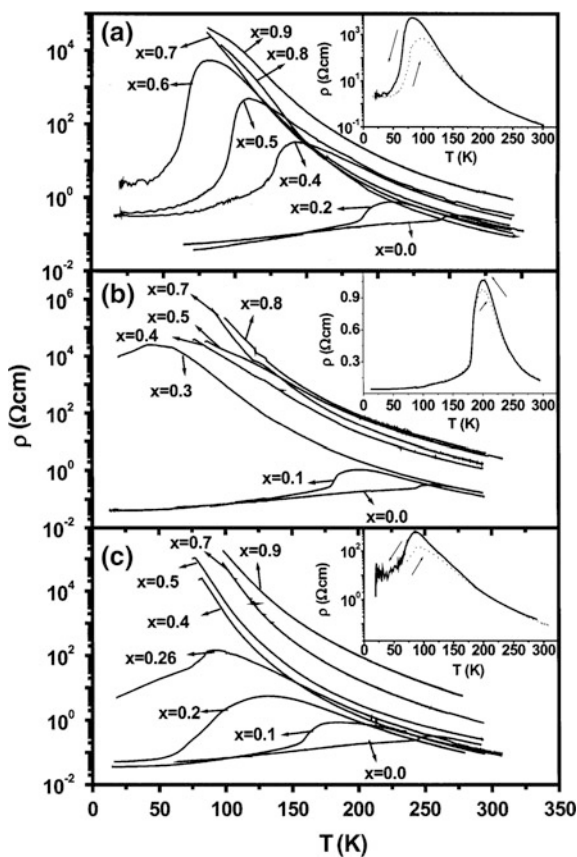
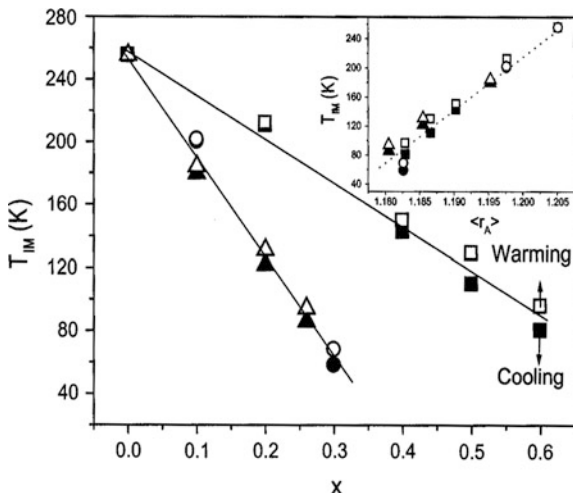


**Fig. 2.4** Temperature-dependent electrical resistivity for  $(\text{La}_{1-x}\text{Ln}_x)_{0.7}\text{Ca}_{0.3}\text{MnO}_3$ . **a** Ln = Nd, **b** Ln = Gd, and **c** Ln = Y. (adapted from Sudheendra et al. [10])

**Fig. 2.5** Plot of  $T_{IM}$  versus  $x$  in  $(La_{1-x}Ln_x)_{0.7}Ca_{0.3}MnO_3$  for  $x \leq x_c$ . The inset shows the variation of  $T_{IM}$  with  $\langle r_A \rangle$  (Å) for the same composition range (adapted from Sudheendra et al. [10])

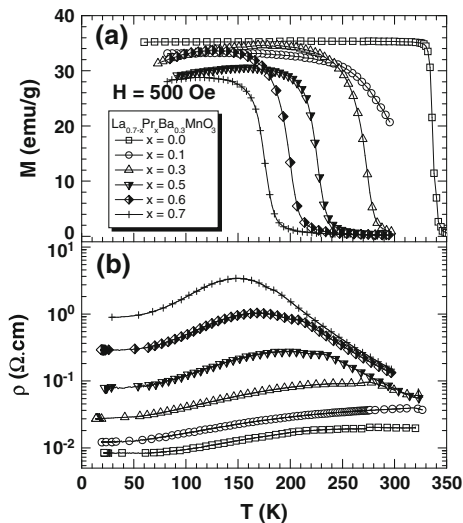


It is useful to examine how these series of perovskites leave the track on the whole magnetic and electrical behaviors and represent a case of EPS. This is corroborated from the results of small but finite magnetic moments and gradually increasing resistivities at low temperatures observed in  $(La_{1-x}Ln_x)_{0.7}Ca_{0.3}MnO_3$  with  $Ln = Pr, Nd, Gd,$  and  $Y$ , around  $x_c$  or  $\langle r_A^c \rangle$ . These are a consequence of electronic phase separation, which also causes thermal hysteresis in the resistivity behavior around  $T_{IM}$  (insets in Fig. 2.4) [10]. The insets in Fig. 2.4a–c show that the resistivity in the warming cycle is lower than that in the cooling cycle up to a certain temperature beyond which the resistivities in the two cycles merge. With decreasing the temperature below the  $T_{IM}$ , the FMM phase grows at the expense of the anti-ferromagnetic insulating phase, causing a decrease in the resistivity value. Whereas during heating, the insulating phase grows at the expense of the FMM phase, the latter provides the conductive path. The thermal hysteresis in the resistivity behavior is therefore due to the percolative conductivity in these magnetic perovskites, the hysteresis decreases with increase in  $\langle r_A \rangle$  or decrease in  $x$  as expected.

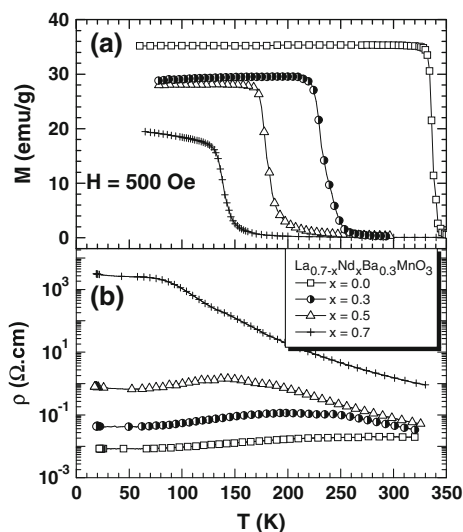
### 2.2.2 Electronic Phase Separation (EPS) in $(La_{1-x}Ln_x)_{0.7}(Ba/Sr)_{0.3}MnO_3$ ( $Ln = Pr, Nd, Gd,$ and $Dy$ )

Figure 2.6 shows the magnetization and resistivity data for  $La_{0.7-x}Pr_xBa_{0.3}MnO_3$  series of magnetic perovskites [15]. The  $T_C$  value decreases progressively with increasing  $x$  and the compound is metallic at room temperature up to  $x = 0.3$  and exhibits a broad I–M transition,  $T_{IM}$ , when  $x \geq 0.3$ . It is interesting that, as  $x$  approaches 0.7, the difference between  $T_C$  and  $T_{IM}$  increases, with the latter becoming considerably lower than  $T_C$ .  $Pr_{0.7}Ba_{0.3}MnO_3$  is, therefore, a ferromagnetic insulator

**Fig. 2.6** Temperature variation of **a** magnetization and **b** electrical resistivity of  $\text{La}_{0.7-x}\text{Pr}_x\text{Ba}_{0.3}\text{MnO}_3$  (adapted from Ref. [15])



**Fig. 2.7** Temperature variation of **a** magnetization and **b** electrical resistivity of  $\text{La}_{0.7-x}\text{Nd}_x\text{Ba}_{0.3}\text{MnO}_3$  (adapted from Ref. [15])



in the regime between  $T_C$  and  $T_{\text{IM}}$  (190–150 K). The magnetization and resistivity data of  $\text{La}_{0.7-x}\text{Nd}_x\text{Ba}_{0.3}\text{MnO}_3$  are shown in Fig. 2.7.

Here again, the  $T_C$  value decreases with increasing  $x$ , and there is a marked decrease in the value of the saturation magnetization as well. There is a sharp increase in magnetization with an apparent  $T_C$  of  $\sim 150$  K, in  $\text{Nd}_{0.7}\text{Ba}_{0.3}\text{MnO}_3$ . But the saturation moment is small, suggesting that there may be no long-range ferromagnetic ordering in the compound and  $\text{Nd}_{0.7}\text{Ba}_{0.3}\text{MnO}_3$  ( $x = 0.7$ ) does not exhibit clear saturation down to low temperatures. The saturation magnetic



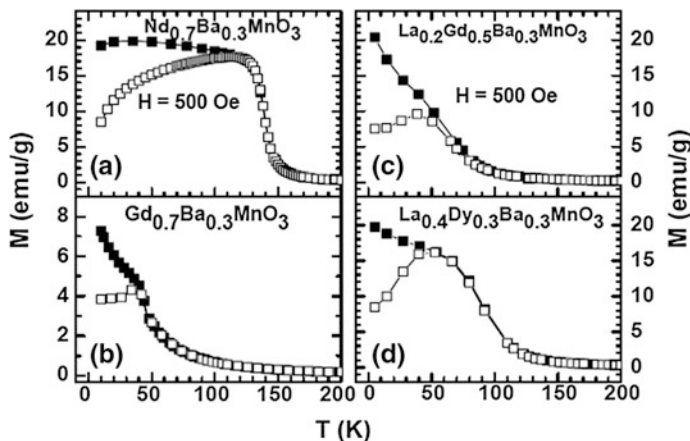


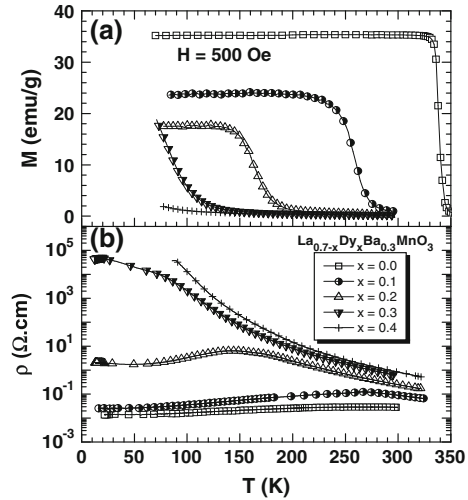
**Fig. 2.8** Temperature variation of the magnetization,  $M$ , of **a**  $\text{Nd}_{0.7}\text{Ba}_{0.3}\text{MnO}_3$  **b**  $\text{Gd}_{0.7}\text{Ba}_{0.3}\text{MnO}_3$  **c**  $\text{La}_{0.2}\text{Gd}_{0.5}\text{Ba}_{0.3}\text{MnO}_3$ , and **d**  $\text{La}_{0.4}\text{Dy}_{0.3}\text{Ba}_{0.3}\text{MnO}_3$  (at  $H = 500$  Oe). The solid symbols represent FC and open symbols represent ZFC data, respectively (adapted from Ref. [15])

moments in  $\text{Nd}_{0.7}\text{Ba}_{0.3}\text{MnO}_3$  and  $\text{La}_{0.7}\text{Ba}_{0.3}\text{MnO}_3$  are  $0.8$  and  $1.5 \mu_B$ , respectively, while that in  $\text{Pr}_{0.7}\text{Ba}_{0.3}\text{MnO}_3$  is  $1.2 \mu_B$ . Accordingly, the ZFC and FC data, show considerable divergence below  $T_C$  (Fig. 2.8a), unlike for the perovskite  $\text{Pr}_{0.7}\text{Ba}_{0.3}\text{MnO}_3$ . The resistivity behavior of  $\text{La}_{0.7-x}\text{Nd}_x\text{Ba}_{0.3}\text{MnO}_3$  is quite different from that of  $\text{La}_{0.7-x}\text{Pr}_x\text{Ba}_{0.3}\text{MnO}_3$ . The  $\text{La}_{0.7-x}\text{Nd}_x\text{Ba}_{0.3}\text{MnO}_3$  compositions show a broad I–M transition when  $x = 0.3$  and  $x = 0.5$ , but the  $0.7$  composition is an insulator with high resistivity.

The resistivity behavior of  $\text{Nd}_{0.7}\text{Ba}_{0.3}\text{MnO}_3$  is different from the literature report [16] to some extent. Since,  $\text{Nd}_{0.7}\text{Ba}_{0.3}\text{MnO}_3$  does not show long-range ferromagnetic ordering; it would appear that the material contains ferromagnetic clusters in the insulating matrix. The double peaks in resistivity data [16] or the shoulder near  $T_C$  also suggest the presence of phase separation. Ferromagnetic clusters in an insulating matrix would also be present in other compositions ( $0.0 < x < 0.7$ ) where  $T_C < T_{IM}$ .

The  $x \geq 0.5$  compositions show divergence between the ZFC and FC magnetization data (Fig. 2.8b, c), indicating the absence of long-range ferromagnetic ordering. AC susceptibility measurements reveal a weakly frequency-dependent peak at  $50$  and  $40$  K, respectively, in the  $x = 0.5$  and  $0.7$  compositions. These compositions also fail to show the I–M transitions in the resistivity data, whereas the samples with  $x < 0.5$  show distinct I–M transitions. The compositions with  $x > 0.5$  are insulating similar to  $\text{Nd}_{0.7}\text{Ba}_{0.3}\text{MnO}_3$  and the resistivity of  $\text{Gd}_{0.7}\text{Ba}_{0.3}\text{MnO}_3$  is higher than that of  $\text{Nd}_{0.7}\text{Ba}_{0.3}\text{MnO}_3$ . In the  $\text{La}_{0.7-x}\text{Dy}_x\text{Ba}_{0.3}\text{MnO}_3$  series, ferromagnetism does not occur for  $x > 0.2$  (Fig. 2.9a). The  $x = 0.2$  composition shows an apparent  $T_C$  of  $180$  K, but the saturation magnetization is very low ( $18$  emu/g). The  $x = 0.2$  composition shows the I–M transition, but all the compositions with  $x > 0.2$  are insulating, the resistivity being higher than

**Fig. 2.9** Temperature variation of **a** magnetization and **b** electrical resistivity of  $\text{La}_{0.7-x}\text{Dy}_x\text{Ba}_{0.3}\text{MnO}_3$  (adapted from Ref. [17])



that of the corresponding Gd- and Nd-substituted magnetic perovskites. The ZFC and FC data of the  $x = 0.3$  composition shows divergence (Fig. 2.8d), indicating the absence of long-range ferromagnetic ordering.

In both the  $\text{La}_{0.7-x}\text{Gd}_x\text{Ba}_{0.3}\text{MnO}_3$  and  $\text{La}_{0.7-x}\text{Dy}_x\text{Ba}_{0.3}\text{MnO}_3$  series of magnetic perovskites, ferromagnetism disappears as  $x$  increases, accompanied by an insulating behavior. The apparent ferromagnetic transitions with a low saturation magnetization observed for  $x = 0.3$  and  $0.2$  at  $150$  and  $180$  K, respectively, in the Gd and Dy derivatives, and associated with  $T_{\text{IM}}$  values lower than  $T_{\text{C}}$ , point to the presence of a ferromagnetic insulating state. It is likely that in all the compositions where the ferromagnetic insulating state occurs, there is phase separation wherein ferromagnetic clusters are present in an insulating matrix. It is interesting that the difference between  $T_{\text{C}}$  and  $T_{\text{IM}}$  manifests itself only when  $\sigma^2$  is considerably large. In  $\text{La}_{0.7-x}\text{Ln}_x\text{Ba}_{0.3}\text{MnO}_3$  series, the difference between  $T_{\text{C}}$  and  $T_{\text{IM}}$  starts emerging when the  $\sigma^2 = 0.016 \text{ \AA}^2$ , although the  $\langle r_{\text{A}} \rangle$  is relatively large, being around  $1.28 \text{ \AA}$ . Clearly, the size disorder plays a crucial role in determining the properties of these magnetic perovskites. The effect of size disorder with constant  $\langle r_{\text{A}} \rangle$  values corresponding to  $\text{Pr}_{0.7}\text{Ba}_{0.3}\text{MnO}_3$  and  $\text{Gd}_{0.7}\text{Ba}_{0.3}\text{MnO}_3$ , respectively, are shown in Figs. 2.10 and 2.11. The  $T_{\text{C}}$  increases with decreasing  $\sigma^2$  and the material becomes metallic at the lowest value of  $\sigma^2 = 0.008 \text{ \AA}^2$ , while I–M transitions occur in the  $\sigma^2$  range of  $0.02\text{--}0.01 \text{ \AA}^2$ . This is indeed a nice result in that a system normally showing an I–M transition becomes metallic as the size disorder is decreased. The effect of size disorder is seen more vividly when the  $\langle r_{\text{A}} \rangle$  value is  $1.216 \text{ \AA}$ , corresponding to  $\text{Gd}_{0.7}\text{Ba}_{0.3}\text{MnO}_3$ , a nonmagnetic insulating material. However, when the size disorder is decreased, the material becomes ferromagnetic, with the  $T_{\text{C}}$  going up to  $\sim 300$  K at the lowest value of  $\sigma^2$  (Fig. 2.11a). As  $\sigma^2$  decreases, the insulating behavior also gives way to metallic behavior.

**Fig. 2.10** Temperature variation of **a** magnetization and **b** the electrical resistivity of  $\text{Ln}_{0.7-x}\text{Ln}'_x\text{A}_{0.3-y}\text{A}'_y\text{MnO}_3$  with a fixed  $\langle r_A \rangle$  value of 1.266 Å (adapted from Ref. [15])

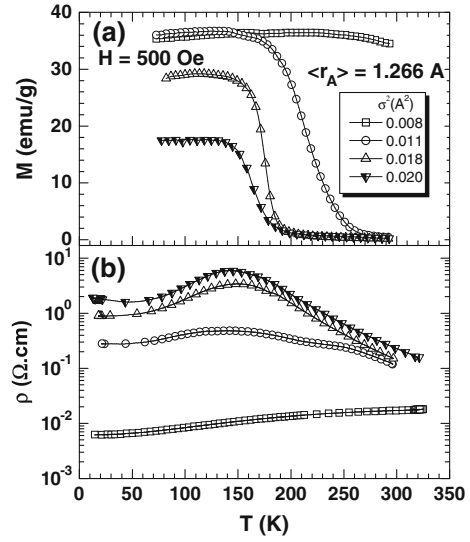
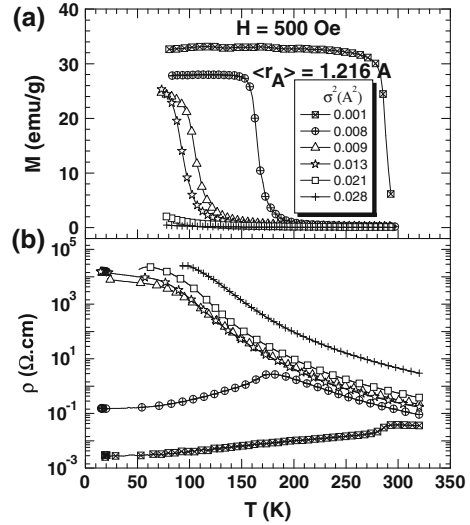
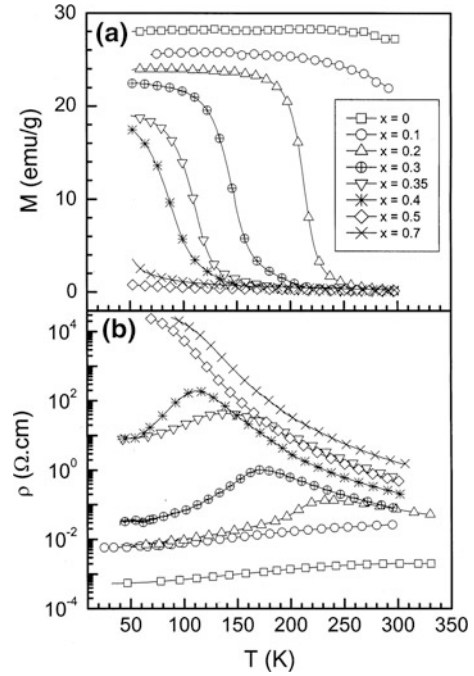


**Fig. 2.11** Temperature variation of **a** magnetization and **b** the electrical resistivity of  $\text{Ln}_{0.7-x}\text{Ln}'_x\text{A}_{0.3-y}\text{A}'_y\text{MnO}_3$  with a fixed  $\langle r_A \rangle$  value of 1.216 Å (adapted from Ref. [15])



The electronic and magnetic properties of  $\text{La}_{0.7-x}\text{Ln}_x\text{Ba}_{0.3}\text{MnO}_3$  ( $\text{Ln} = \text{Pr}, \text{Nd}, \text{Gd}, \text{and Dy}$ ) magnetic perovskites have revealed certain interesting aspects, wherein the average radius of the A-site cation generally remains large (1.216–1.292 Å), but the size disorder is considerable. Since the band narrowing due to small  $\langle r_A \rangle$  is avoided, the predominant effect in these materials is due to size disorder. It is interesting that these materials show a progressive decrease in the FM  $T_C$ , eventually giving rise to a non-FM insulating behavior. Accordingly, with

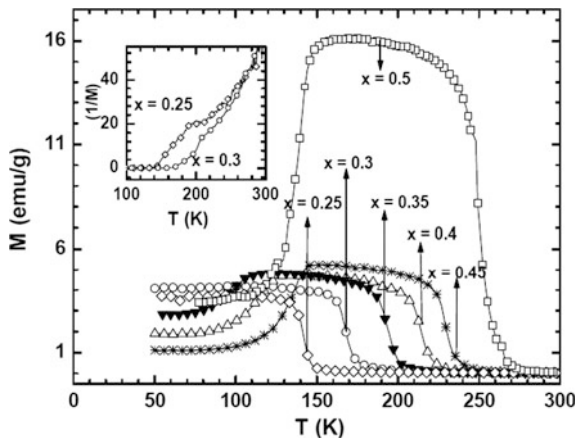
**Fig. 2.12** Temperature variation of **a** magnetization and **b** resistivity of  $\text{La}_{0.7-x}\text{Dy}_x\text{Sr}_{0.3}\text{MnO}_3$  (adapted from Ref. [15])



increasing  $x$  or  $\sigma^2$ , the material exhibits a ferromagnetic insulating phase due to the presence of FM clusters in the insulating matrix. At large  $x$  or  $\sigma^2$ , where some of the compositions lose ferromagnetism and become insulating, there is evidence for clusters with short-range FM interaction. In the insulating regime caused by size disorder, there is clearly phase separation due to the presence of FM clusters in an insulating matrix. The phase separation is minimized or eliminated by decreasing  $\sigma^2$ , as evidenced from the change of the nonmagnetic insulating phase to an FM metallic state.

In Fig. 2.12 we show the magnetization and resistivity data of  $\text{La}_{0.7-x}\text{Dy}_x\text{Sr}_{0.3}\text{MnO}_3$ . The  $T_C$  values decrease with increasing  $x$  up to a composition  $x_c \sim 0.4$ . The value of  $T_C$  decreases from 350 K for  $x = 0.0$  to  $\sim 110$  K for  $x = 0.4$ . The abrupt change in magnetization of  $\text{La}_{0.7-x}\text{Dy}_x\text{Sr}_{0.3}\text{MnO}_3$  is noteworthy. There is a small increase in the magnetization at low temperatures ( $\leq 80$  K) in the  $x > x_c$  compositions (Fig. 2.12a), but this is not due to long-range FM ordering. If these compositions were FM the  $T_C$  value would be expected much higher based on the  $\langle r_A \rangle$  value. When  $x > x_c$ , the materials are no longer FM and accordingly, the resistivity increases with the decrease in temperature, as in insulator (Fig. 2.12b). At large  $x$  ( $x > x_c$ )  $\text{La}_{0.7-x}\text{Dy}_x\text{Sr}_{0.3}\text{MnO}_3$  ceases to exhibit ferromagnetism and I-M transition, and instead becomes an insulator with a small increase in magnetization at low temperature indicating that the FM clusters occur in a paramagnetic matrix. The large change in the properties around  $x_c$  reflects the presence of electronic phase separation in the Sr-substituted magnetic perovskites as well.

**Fig. 2.13** Temperature variation of magnetization of  $\text{Nd}_{0.5}\text{Ca}_{0.5-x}\text{Sr}_x\text{MnO}_3$ . The *inset* shows the variation of inverse magnetization with temperature, adapted from Ref. [17]



### 2.2.3 Electronic Phase Separation (EPS) in $\text{Nd}_{0.5}\text{Ca}_{0.5-x}\text{Sr}_x\text{MnO}_3$ ( $x = 0-0.5$ )

The  $\text{Nd}_{0.5}\text{Ca}_{0.5-x}\text{Sr}_x\text{MnO}_3$  perovskites [17] show the well-known ferromagnetic transition around 250 K and undergo charge-ordering transition on cooling at 150 K when  $x = 0.5$ , the material becoming antiferromagnetic around the same temperature (Fig. 2.13). Both the ferromagnetic and charge-ordering transitions are sharp in this composition. The  $x = 0$  composition ( $\text{Nd}_{0.5}\text{Ca}_{0.5}\text{MnO}_3$ ) shows only charge ordering ( $T_{\text{CO}} = 240$  K) but no ferromagnetism. The  $\text{Nd}_{0.5}\text{Ca}_{0.5-x}\text{Sr}_x\text{MnO}_3$ , compositions with  $x = 0.25-0.45$  show ferromagnetic transitions (Fig. 2.13), with the  $T_{\text{C}}$  increasing with increase in  $x$  and the  $x = 0.25$  composition has a  $T_{\text{C}}$  close to 150 K. However, it is noteworthy that when  $x < 0.35$ , there is no sharp drop in magnetization data corresponding to the charge-ordering transition. The compositions with  $x = 0.25$  and  $0.30$  are more like  $\text{Nd}_{0.5}\text{Ca}_{0.5}\text{MnO}_3$  and the temperature variation of the inverse magnetization shows a dip corresponding to  $T_{\text{CO}}$  (inset Fig. 2.13).

The occurrence of a phase-separated state below  $T_{\text{CO}}$  ( $T_{\text{N}}$ ) in some of the manganate compositions was pointed out earlier. The situation is even more complex in  $\text{Nd}_{0.5}\text{Sr}_{0.5}\text{MnO}_3$ . High-resolution X-ray and neutron diffraction investigations show that  $\text{Nd}_{0.5}\text{Sr}_{0.5}\text{MnO}_3$  separates into three macroscopic phases at low temperatures [17]. The phases involved are the high-temperature FMM phase, the orbitally ordered A-type AFM phase, and the charge-ordered CE-type AFM phase. On cooling the manganite, the A-type AFM phase starts manifesting itself around 220 K, with the charge-ordered AFM phases appearing at 150 K. At the so-called FM metallic-CO AFM transition, all the three phases coexist, and this situation continues down to very low temperatures as shown in Fig. 2.14.

**Fig. 2.14** Variation in the percentage of the different phases of  $\text{Nd}_{0.5}\text{Sr}_{0.5}\text{MnO}_3$  with temperature (adapted from Ref. [17])

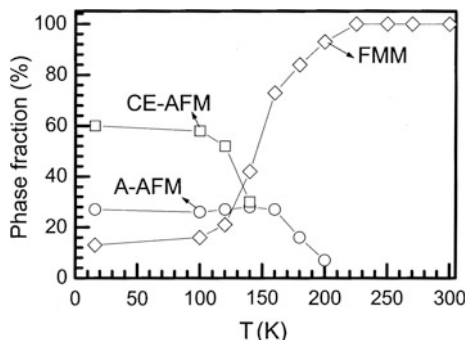


**Fig. 2.15** Schematic diagram of the percentage volume fractions of different phases of  $\text{Nd}_{0.5}\text{Sr}_{0.5}\text{MnO}_3$  under **a**  $H = 0$  T and **b** 6 T (adapted from Ref. [18])

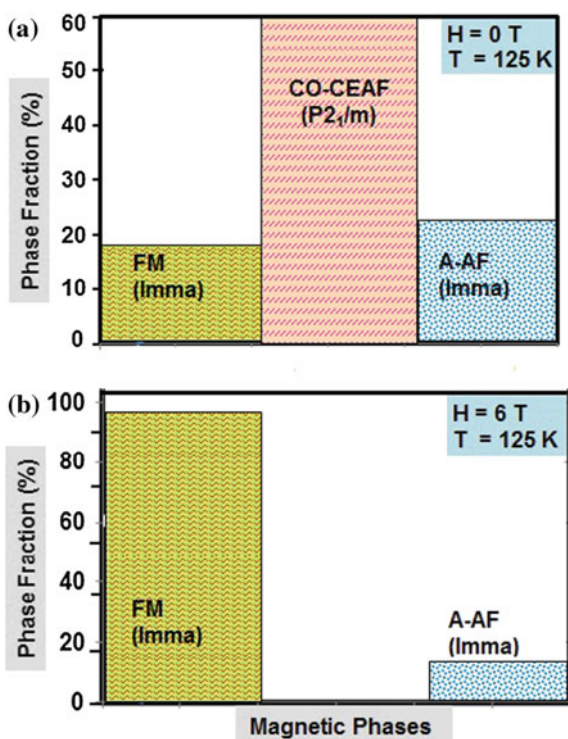
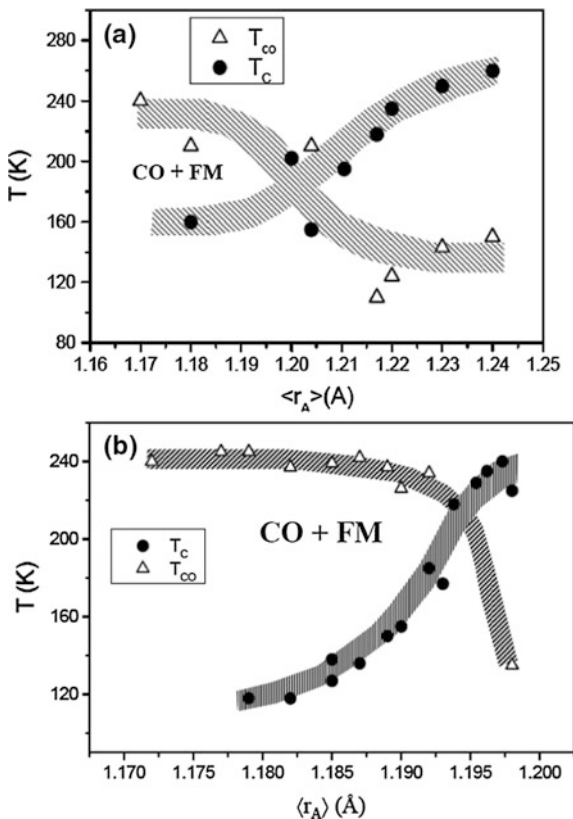


Figure 2.15 shows the percentage volume fraction of the different phases in the presence and absence of a magnetic field [18]. Phase separation in this system seems to depend crucially on the  $\text{Mn}^{4+}/\text{Mn}^{3+}$  ratio, a ratio slightly greater than unity stabilizes the A-type AFM phases. Thus,  $\text{Nd}_{0.45}\text{Sr}_{0.55}\text{MnO}_3$  has the A-type AFM structure.

Figure 2.16 shows the  $T_C$  and  $T_{CO}$  values in the  $\text{Nd}_{0.5}\text{Ca}_{0.5-x}\text{Sr}_x\text{MnO}_3$  and  $\text{La}_{0.5-x}\text{Ln}_x\text{Ca}_{0.5}\text{MnO}_3$  ( $\text{Ln} = \text{Pr}, \text{Nd}$ ) series against  $\langle r_A \rangle$ . Although there is some scatter in the points, the data indicate that when  $\langle r_A \rangle \sim 1.20$  Å, the  $T_C < T_{CO}$ ,

**Fig. 2.16** Variation of the FM Curie temperature,  $T_C$ , and the charge-ordering transition temperature,  $T_{CO}$ , with  $\langle r_A \rangle$  in **a**  $\text{Nd}_{0.5}\text{Ca}_{0.5-x}\text{Sr}_x\text{MnO}_3$  and **b**  $\text{La}_{0.5-x}\text{Ln}_x\text{Ca}_{0.5}\text{MnO}_3$  ( $\text{Ln} = \text{Pr}, \text{Nd}$ ). In the temperature range between  $T_{CO}$  and  $T_C$ , the charge-ordered and FM phases coexist (adapted from Ref. [19])

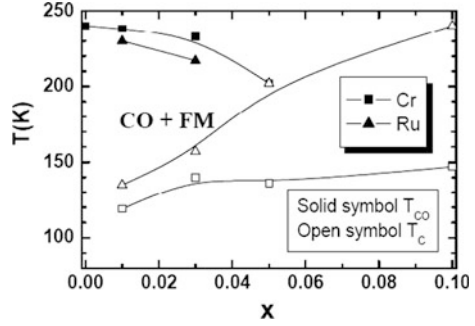


suggesting that the ferromagnetic transition is reentrant in nature [19]. Furthermore, the  $T_C$ - $\langle r_A \rangle$  and  $T_{CO}$ - $\langle r_A \rangle$  curves cross each other around  $\langle r_A \rangle = 1.20$  Å. It is likely that over the entire  $\langle r_A \rangle$  range 1.17–1.24 Å, there is coexistence of the CO and FM phases, especially in the temperature range between  $T_{CO}$  and  $T_C$ . In Fig. 2.17, we have shown the data for  $\text{Nd}_{0.5}\text{Ca}_{0.5}\text{Mn}_{1-x}\text{M}_x\text{O}_3$  ( $\text{M} = \text{Cr}, \text{Ru}$ ) series, where  $\langle r_A \rangle$  is constant (1.17 Å) [20]. The  $T_{CO}$  generally decreases with increase in  $x$ , while  $T_C$  increases specially in the case of Ru substitution. It appears that this ferromagnetic transition is reentrant in nature in these magnetic perovskites and suggests that  $T_C$  and  $T_{CO}$  curves cross each other at a specific value of  $x$ . In the temperature range between  $T_{CO}$  and  $T_C$ , the charge-ordered and FM phases coexist.

In perovskite manganites, the reason behind the value  $T_{CO} > T_C$  with small  $\langle r_A \rangle$  ( $\langle r_A \rangle < 1.20$  Å) is probably because of electronic phase separation. It is known that only when  $\langle r_A \rangle < 1.20$  or 1.19 Å, charge ordering and associated effects occur in the perovskite manganites [9, 10]. The so-called FM transition is thus a consequence of electronic phase separation. The  $T_C$ 's at small  $\langle r_A \rangle$  do not really correspond to genuine FM transitions, and accordingly the saturation magnetization values of these samples at low temperatures are small. It is only at large  $\langle r_A \rangle$ , ( $\langle r_A \rangle \geq 1.20$  Å) that genuine FM phases associated with high  $T_C$  values get manifested.



**Fig. 2.17** Variation of ferromagnetic Curie temperature,  $T_C$ , and the CO transition temperature,  $T_{CO}$ , with  $x$  in  $\text{Nd}_{0.5}\text{Ca}_{0.5}\text{Mn}_{1-x}\text{M}_x\text{O}_3$  ( $M = \text{Cr}, \text{Ru}$ ) (adapted from Ref. [20])



The magnetic and electron transport properties of these magnetic perovskites could be understood in terms of electronic phase separation. The system becomes FM metallic on cooling the CO insulating state and this behavior is favored for small  $\langle r_A \rangle$  value. In these systems, the  $T_C$  increases with increase in  $\langle r_A \rangle$  while  $T_{CO}$  decreases and accordingly the crossover between  $T_{CO}$  and  $T_C$  takes place around  $\langle r_A \rangle$  value of 1.195 and 1.20 Å for two series of manganites. It appears that in the intermediate temperature range between  $T_{CO}$  and  $T_C$ , the FM metallic and CO insulating phases coexist for these compositions and such electronic phase separation is expected to be favored by small  $\langle r_A \rangle$  values.

#### 2.2.4 Electronic Phase Separation (EPS) in $\text{Pr}_{1-x}\text{Ca}_x\text{MnO}_3$ ( $X = 0.3-0.4$ )

The studies of neutron scattering and diffraction by Radaelli et al. [4, 5] have shown tunable mesoscopic phase separation in  $\text{Pr}_{0.7}\text{Ca}_{0.3}\text{MnO}_3$ . Intragranular strain-driven mesoscopic phase separation (5–20 nm) between two insulating phases (one charge-ordered and another spin glass) occurs below  $T_{CO}$ . The charge-ordered phase orders antiferromagnetically and the other remains a spin glass. On the application of a high magnetic field, most of the material goes to a FM state. Microscopic phase separation (0.5–2 nm) is present at all temperatures, especially in the spin glass phase at low temperatures. Electric fields produce interesting effects on  $\text{Pr}_{0.6}\text{Ca}_{0.4}\text{MnO}_3$  and similar CO magnetic perovskites.

In Fig. 2.18, we show the effect of electric currents on the resistivity of  $\text{Pr}_{0.6}\text{Ca}_{0.4}\text{MnO}_3$  and  $\text{Nd}_{0.5}\text{Ca}_{0.5}\text{MnO}_3$  crystals when the sample is cool down to 15 K from 300 K. There are four distinct features in the plots. There is a drop in the resistivity throughout the temperature range as the current,  $I$ , is increased. The temperature dependence of resistivity changes with the increase in  $I$ . An insulator–metal transition occurs around 60 K ( $T_{IM}$ ) at high values of  $I$ , beyond a threshold value. The change in the resistivity is not due to Joule heating as evidenced from the



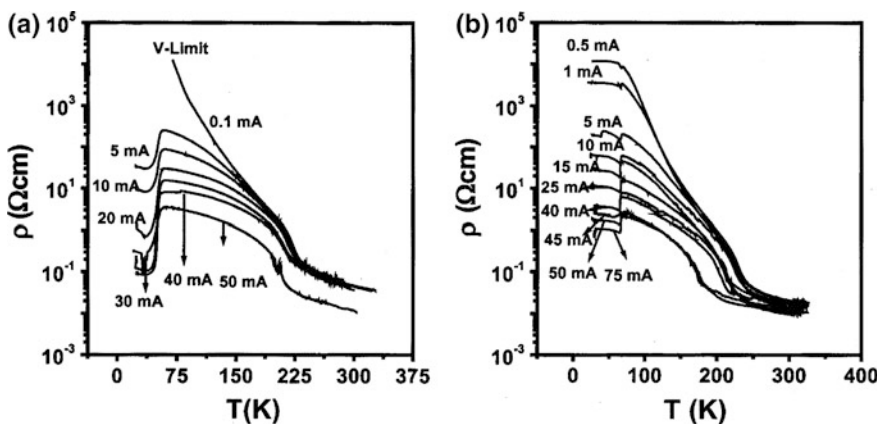


**Fig. 2.18** Temperature variation of electrical resistivity of **a**  $\text{Pr}_{0.6}\text{Ca}_{0.4}\text{MnO}_3$  and **b**  $\text{Nd}_{0.5}\text{Ca}_{0.5}\text{MnO}_3$  for different values of current (adapted from Rao et al. [8])

negative thermal coefficient of resistivity at high temperatures and the change in sign at the I–M transition [8]. The negative differential resistance, i.e., the decrease in resistivity with increase in current observed beyond a certain value of  $I$  (Fig. 2.18), is due to the presence of the metallic filaments, which are ferromagnetic and carry most of the current [8]. The rather high value of the resistivity below the transition temperature is attributed to the coexistence of the FM and CO insulator phases. The relative fraction of the FMM phase increases with increasing current causing a lowering of resistivity below the  $T_{\text{IM}}$  [8]. The small rise in resistivity below the I–M transition may be attributed to the tunneling of electrons between the FMM clusters through COI clusters.

### 2.2.5 Glassy Ferromagnetism in $\text{Ln}_{0.7}\text{Ba}_{0.3}\text{MnO}_3$ ( $\text{Ln} = \text{La}, \text{Nd}, \text{and Gd}$ )

We have discussed earlier that the perovskite manganites  $(\text{La}_{1-x}\text{Tb}_x)_{0.67}\text{Ca}_{0.33}\text{MnO}_3$  is FMM for lower doping  $x$  and spin glass at large  $x$  ( $\geq 0.33$ ). In this section we will discuss for  $\text{Ln}_{0.7}\text{Ba}_{0.3}\text{MnO}_3$  manganites in this direction. Figure 2.19 shows the magnetization and resistivity behavior of  $\text{La}_{0.7}\text{Ba}_{0.3}\text{MnO}_3$ ,  $\text{Nd}_{0.7}\text{Ba}_{0.3}\text{MnO}_3$  and  $\text{Gd}_{0.7}\text{Ba}_{0.3}\text{MnO}_3$  [15]. Clearly, the magnetic properties of the three perovskites are distinctly different from one another.  $\text{La}_{0.7}\text{Ba}_{0.3}\text{MnO}_3$  shows FMM behavior below  $T_{\text{C}}$ , whereas  $\text{Nd}_{0.7}\text{Ba}_{0.3}\text{MnO}_3$  and  $\text{Gd}_{0.7}\text{Ba}_{0.3}\text{MnO}_3$  show insulating behavior with complex magnetism. Figure 2.20 shows the low-field ZFC and FC magnetization data of  $\text{Nd}_{0.7}\text{Ba}_{0.3}\text{MnO}_3$  and  $\text{Gd}_{0.7}\text{Ba}_{0.3}\text{MnO}_3$ , the later one  $\text{Gd}_{0.7}\text{Ba}_{0.3}\text{MnO}_3$  exhibits a rather complex behavior below 62 K.

It is noteworthy that there are three characteristic temperatures: 62 K (onset of significant irreversibility between the ZFC and FC magnetization curves), 46 K

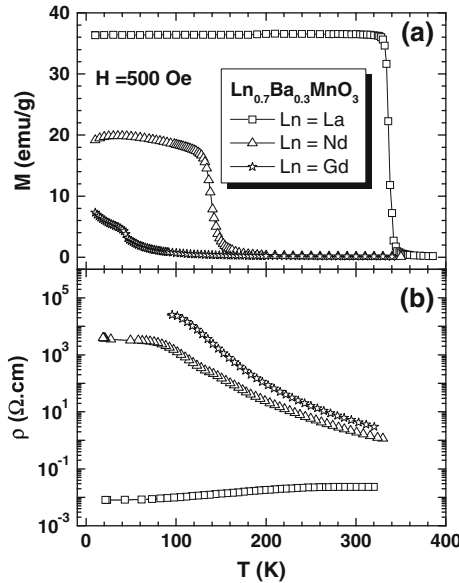


**Fig. 2.19** Temperature dependence of **a** the FC magnetization,  $M$ , (at  $H = 500$  Oe) and **b** the electrical resistivity,  $\rho$ , of  $\text{Ln}_{0.7}\text{Ba}_{0.3}\text{MnO}_3$  with  $\text{Ln} = \text{La}$ ,  $\text{Nd}$ , and  $\text{Gd}$ . Note that  $\text{Nd}_{0.7}\text{Ba}_{0.3}\text{MnO}_3$  is insulating at 150 K where there is weak magnetic transition (adapted from Ref. [15])

(a maximum in the FC curve), and 36 K (a maximum in the ZFC curve), all indicating different ordering and/or freezing processes in the system. The field variation of magnetization at different temperatures for  $\text{Nd}_{0.7}\text{Ba}_{0.3}\text{MnO}_3$  shows a behavior similar to a soft ferromagnet. However,  $\text{Gd}_{0.7}\text{Ba}_{0.3}\text{MnO}_3$  does not show a ferromagnet at low temperatures, and exhibit no saturation even at high fields. The shape of the  $M$ - $H$  curve and the absence of saturation even at high fields found in  $\text{Gd}_{0.7}\text{Ba}_{0.3}\text{MnO}_3$  are reminiscent of magnetization curves of spin glasses [21].

Figure 2.21 shows the in-phase  $\chi'(T)$  component of the AC susceptibility, which reveals similar features as the ZFC magnetization at low field in both the manganites.  $\text{Nd}_{0.7}\text{Ba}_{0.3}\text{MnO}_3$  shows a sharp frequency-independent maximum below 150 K. However, there is weak frequency dependence at temperatures below 140 K, a behavior similar to  $\text{Nd}_{0.7}\text{Sr}_{0.3}\text{MnO}_3$  [22].  $\text{Gd}_{0.7}\text{Ba}_{0.3}\text{MnO}_3$  shows a shoulder around 62 K, a weak anomaly just above 46 K and a maximum at 36 K. The  $\chi'(T)$  data become strongly frequency dependent below 36 K. This transition could arise from the presence of small magnetic clusters in a nonmagnetic matrix. Time-dependent ZFC magnetization measurements show that both  $\text{Nd}_{0.7}\text{Ba}_{0.3}\text{MnO}_3$  and  $\text{Gd}_{0.7}\text{Ba}_{0.3}\text{MnO}_3$  exhibit logarithmically slow dynamics and aging at low temperatures (Fig. 2.22).

Magnetic aging is a signature of spin glasses and explained within the droplet (or domain growth) model the maximum in the relaxation rate is associated with a crossover between quasi-equilibrium and nonequilibrium dynamics. The slow

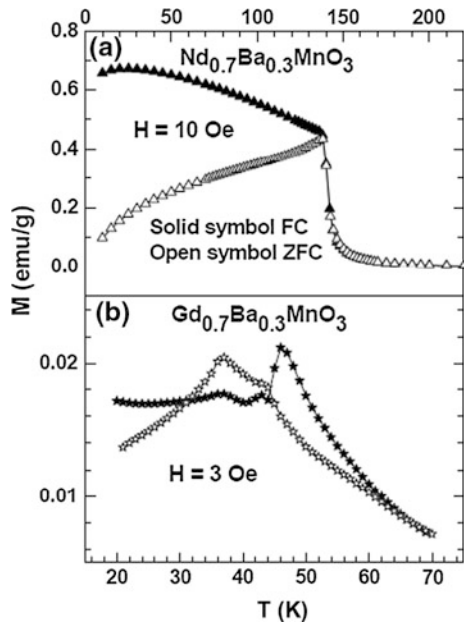
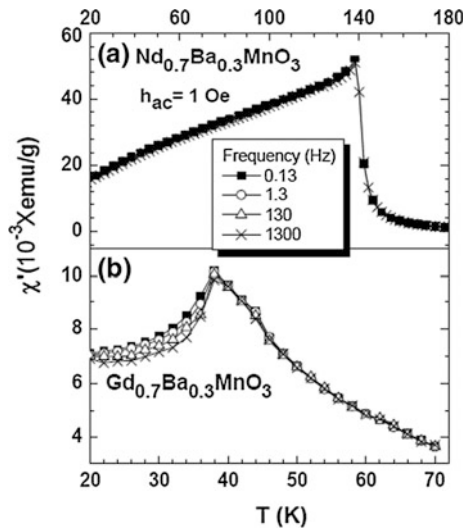


**Fig. 2.20** Temperature-dependent magnetization for **a**  $\text{Nd}_{0.7}\text{Ba}_{0.3}\text{MnO}_3$  (at  $H = 10$  Oe) and **b**  $\text{Gd}_{0.7}\text{Ba}_{0.3}\text{MnO}_3$  (at  $H = 3$  Oe) (adapted from Ref. [15])

**Fig. 2.21** Temperature dependence of the in-phase AC susceptibility at different frequencies for **a**  $\text{Nd}_{0.7}\text{Ba}_{0.3}\text{MnO}_3$  and **b**  $\text{Gd}_{0.7}\text{Ba}_{0.3}\text{MnO}_3$  (adapted from Ref. [15])



relaxation and aging behavior of  $\text{Nd}_{0.7}\text{Ba}_{0.3}\text{MnO}_3$  and  $\text{Gd}_{0.7}\text{Ba}_{0.3}\text{MnO}_3$  demonstrate that magnetic disorder and frustration occur in the low temperature phases. Glassy dynamics in spin glasses is also manifested by a memory effect that can be

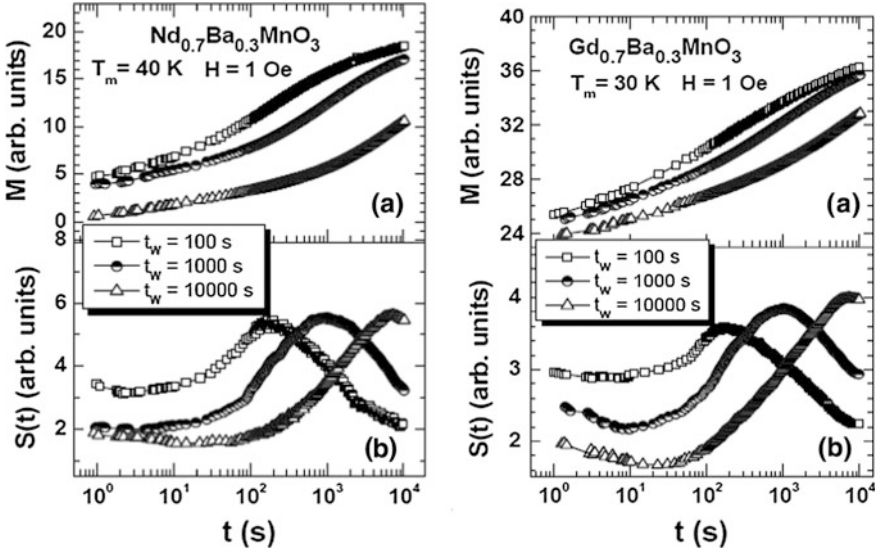


**Fig. 2.22** ZFC-relaxation measurements for  $\text{Nd}_{0.7}\text{Ba}_{0.3}\text{MnO}_3$  and  $\text{Gd}_{0.7}\text{Ba}_{0.3}\text{MnO}_3$  for different waiting times (adapted from Ref. [15])

demonstrated by DC magnetization or low frequency AC susceptibility experiments. In a spin glass experiment, the memory curve acquires a weak dip at the temperature where the zero-field cooling was halted. A spin glass phase (ordinary or reentrant) has a pronounced memory behavior, whereas a disordered and frustrated ferromagnetic phase shows little or no memory effect. Figure 2.23a shows the memory curve, reveals a broad but shallow memory of the stop at 120 K.

In contrast, the corresponding experiment on the  $\text{Gd}_{0.7}\text{Ba}_{0.3}\text{MnO}_3$  sample shows a prominent memory dip. There is a significant difference between the reference and

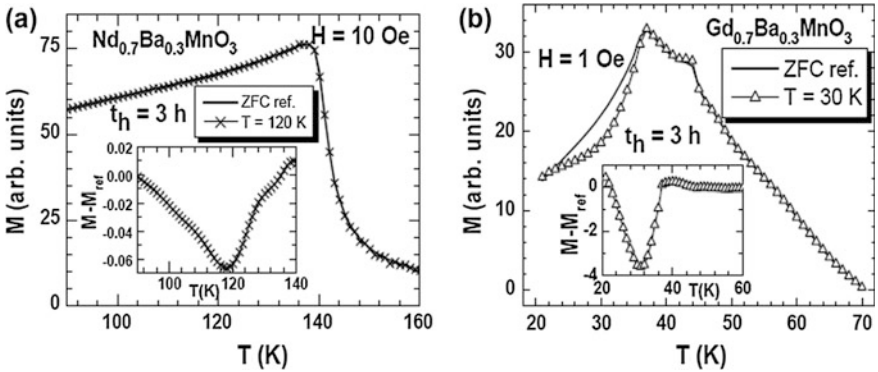


**Fig. 2.23** ZFC-magnetization memory experiments for **a**  $\text{Nd}_{0.7}\text{Ba}_{0.3}\text{MnO}_3$  and **b**  $\text{Gd}_{0.7}\text{Ba}_{0.3}\text{MnO}_3$  (adapted from Ref. [15])

the memory curves, with a broad memory dip. The dip abruptly ceases above 36 K, hence the memory behavior of  $\text{Gd}_{0.7}\text{Ba}_{0.3}\text{MnO}_3$  at 36 K signifies spin glass behavior.  $\text{Nd}_{0.7}\text{Ba}_{0.3}\text{MnO}_3$  shows a pronounced aging behavior, but a rather weak memory effect below 150 K, probably due to the presence of FM clusters in an insulating matrix. It appears to be a cluster glass or a magnetically disordered system.  $\text{Gd}_{0.7}\text{Ba}_{0.3}\text{MnO}_3$  appears to contain small magnetic clusters, giving rise to a spin glass state below 36 K. The behavior of  $\text{Gd}_{0.7}\text{Ba}_{0.3}\text{MnO}_3$  is attributed to the large size mismatch between the A-site cations or large  $\sigma^2$  value ( $0.028 \text{ \AA}^2$ ), the mismatch being considerably smaller in  $\text{Nd}_{0.7}\text{Ba}_{0.3}\text{MnO}_3$ . Such size mismatch favors chemical/electronic inhomogeneities, this is a unique case of a perovskite manganite showing a size disorder-induced spin glass behavior, occurring in spite of the relatively large A-site cation radius ( $\langle r_A \rangle = 1.216 \text{ \AA}$ ). The FM insulating state or nonmagnetic insulating state often reported in the rare earth manganites of the type  $\text{Ln}_{1-x}\text{A}_x\text{MnO}_3$  arises from the glassy behavior of the magnetic clusters in these materials, generally associated with electronic phase separation [2–8].

### 2.3 Cobalt-Centered Magnetic Perovskites

The physical properties of perovskite cobaltites  $\text{Ln}_{1-x}\text{A}_x\text{CoO}_3$  (Ln = rare earth, A = alkaline earth) are somewhat similar to that of the perovskite manganites, unlike the spin state transitions in the case of perovskite cobaltites [23, 24]. One of the fundamental aspects of the transition metal chemistry is ligand field theory, which provides the possible explanation for the spin state transitions of perovskite cobaltites. In this section we have discussed the effect of A-site cation and size disorder on the magnetic and electrical properties as well as the factors that influence the EPS and spin glass behavior. Recently, Phelan et al. [24] have reported the EPS and MR effect in perovskite cobaltites  $\text{Pr}_{0.5}\text{Ca}_{0.5}\text{CoO}_{3-\delta}$  and  $(\text{Pr}_{1-y}\text{Y}_y)_{1-x}\text{Ca}_x\text{CoO}_{3-\delta}$ , where the ground state is a magnetically and electronically inhomogeneous state characterized by FM clusters (on a broad spectrum of length scales) embedded in a non-FM matrix. The clusters have a mean correlation length of  $50 \text{ \AA}$  at 4 K, although magnetic inhomogeneity occurs across a broad spectrum of length scales, evidenced by a highly inhomogeneous ground state. This magnetically inhomogeneous state manifests an intercluster magnetoresistance effect, which is a phenomenon of importance in understanding the CMR effect in perovskite cobaltites as well as for manganites. In terms of electronic properties, generally the perovskite cobaltites have insulating/semiconducting ground states. He et al. [24] have reported finite spin states, formation of ferromagnetic droplets (of nanometers in size), and a magneto-electronically phase-separated state characterized by FM clusters embedded in a non-FM matrix over a doping range  $0.04 < x < 0.22$  in  $\text{La}_{1-x}\text{Sr}_x\text{CoO}_{3-\delta}$ . For  $x > 0.22$  on the other hand, behaves as a uniform FM metal [24].

### 2.3.1 Electronic Phase Separation in $\text{La}_{0.7-x}\text{Ln}_x\text{Ca}_{0.3}\text{CoO}_3$ ( $\text{Ln} = \text{Pr}, \text{Nd}, \text{Gd}, \text{and Dy}$ )

Figure 2.24 shows the result of magnetic measurements for the  $\text{La}_{0.7-x}\text{Ln}_x\text{Ca}_{0.3}\text{CoO}_3$  perovskites with ( $\text{Ln} = \text{La}, \text{Pr}, \text{Nd}$ ), which signifies how the magnetic transition is sensitive to the substitution of the smaller cations in place of rare earth  $\text{La}^{3+}$ .  $\text{La}_{0.7}\text{Ca}_{0.3}\text{CoO}_3$  exhibits a ferromagnetic transition ( $T_C \sim 175 \text{ K}$ ),  $\text{Pr}_{0.7}\text{Ca}_{0.3}\text{CoO}_3$  and  $\text{Nd}_{0.7}\text{Ca}_{0.3}\text{CoO}_3$  do not show distinct ferromagnetic transitions [23].

There is a slight increase in the susceptibility of  $\text{Pr}_{0.7}\text{Ca}_{0.3}\text{CoO}_3$  around 75 K, but this is not due to a genuine ferromagnetic transition. On the basis of the  $\langle r_A \rangle$  values, the ferromagnetic  $T_C$ 's of  $\text{Pr}_{0.7}\text{Ca}_{0.3}\text{CoO}_3$  and  $\text{Nd}_{0.7}\text{Ca}_{0.3}\text{CoO}_3$  expected to

**Fig. 2.24** Temperature dependence of magnetization for  $\text{La}_{0.7-x}\text{Ln}_x\text{Ca}_{0.3}\text{CoO}_3$  with **a**  $\text{Ln} = \text{Pr}$  and **b**  $\text{Ln} = \text{Nd}$ . ZFC data in broken curves and FC data in solid curves (at 1 kOe) (adapted from Ref. [23])

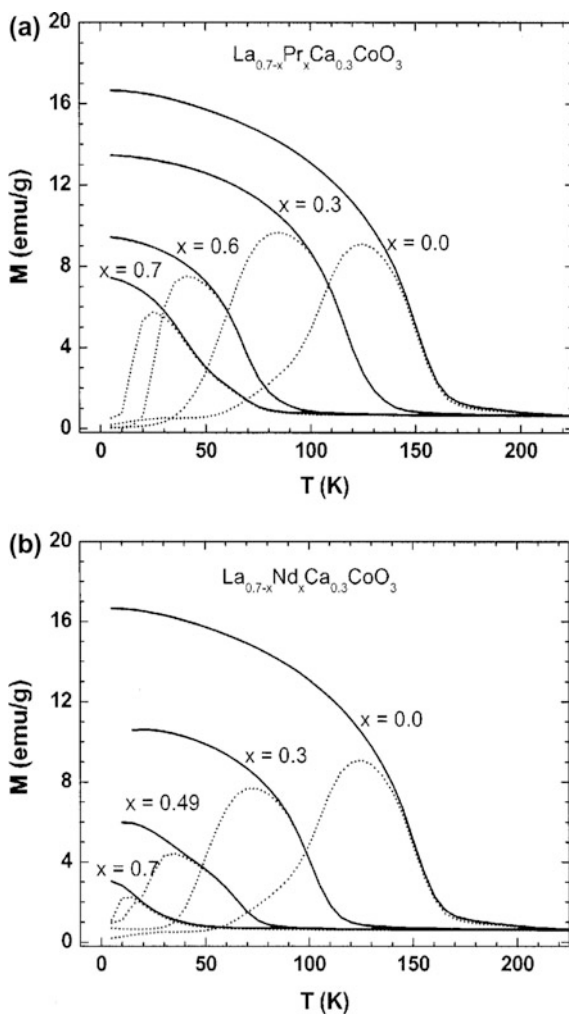
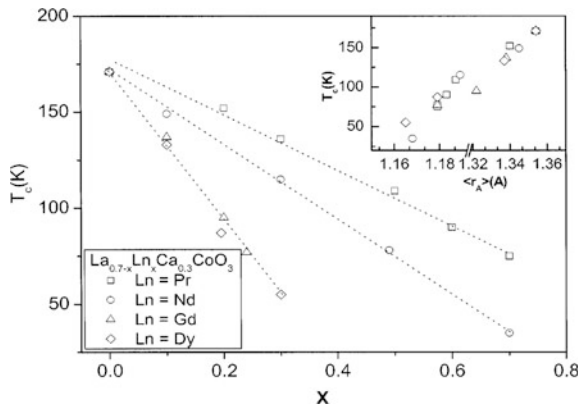


**Fig. 2.25** Variation of the ferromagnetic  $T_C$  with  $x$  in  $\text{La}_{0.7-x}\text{Ln}_x\text{Ca}_{0.3}\text{CoO}_3$ . The inset shows the variation of  $T_C$  with  $\langle r_A \rangle$  (Å) (adapted from Ref. [23])



be well above 100 K. The FM  $T_C$  values in the four series of perovskite cobaltites are plotted against  $x$  in Fig. 2.25. The  $T_C$  value decreases linearly with increasing  $x$ .

The  $M(H)$  hysteresis curves do not show saturation in all the compositions. The absence of saturation is a characteristic of a glassy system. Furthermore, the remanent magnetization,  $M_r$ , decreases with increase in  $x$  or decrease in  $\langle r_A \rangle$ . The magnetization,  $M$ , and  $M_r$  increase with  $\langle r_A \rangle$ , but their values become rather low when  $\langle r_A \rangle \leq 1.18$  Å (Fig. 2.26).

The electrical resistivities of the perovskite cobaltites show similar trends to the magnetic properties. Figure 2.27 shows resistivity for two series of perovskite

**Fig. 2.26** Variation of **a** the magnetic moment,  $\mu_B$ , **b** remanent magnetization,  $M_r$ , and **c** the electrical resistivity in  $\text{La}_{0.7-x}\text{Ln}_x\text{Ca}_{0.3}\text{CoO}_3$  with  $\langle r_A \rangle$  (Å) (50 K) (adapted from Ref. [23])

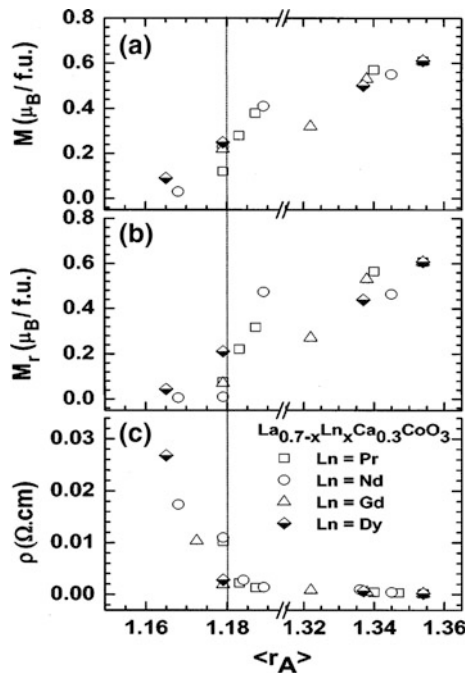
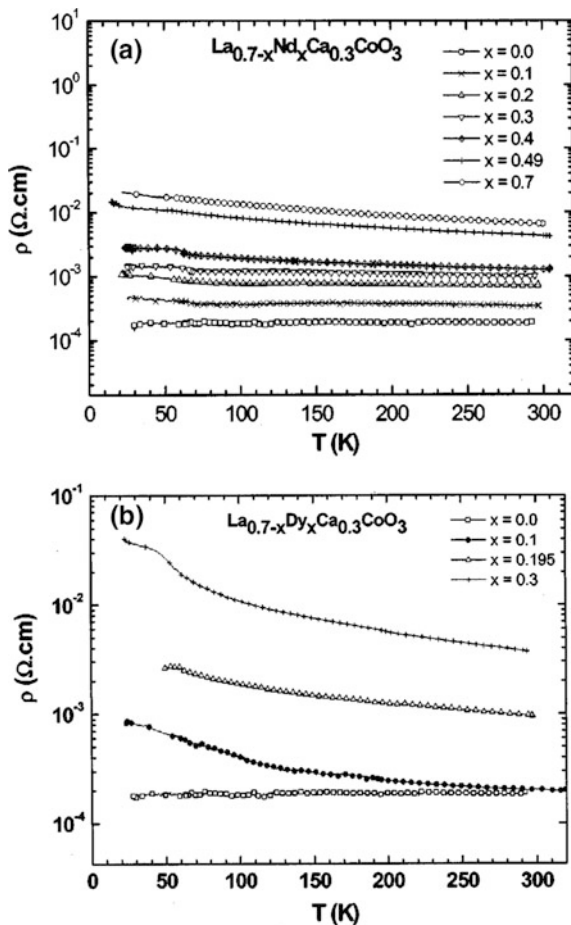


**Fig. 2.27** Temperature variation of the electrical resistivity of  $\text{La}_{0.7-x}\text{Ln}_x\text{Ca}_{0.3}\text{CoO}_3$  (Ln = Nd and Dy) (adapted from Ref. [23])



cobaltites. The temperature coefficient of resistivity changes from a near-zero value to a negative value around  $x_c$  in some of the series, but in all the four series the magnitude of resistivity shows a marked increase around a critical composition  $x_c$  or a critical radius  $\langle r_A^c \rangle$  of  $\sim 1.18$  Å. We noticed this behavior at  $x = 0.490$  and  $0.195$  for the Nd and Dy series, respectively (Fig. 2.27). In order to rationalize the resistivity data in the four series of perovskite cobaltites, we have plotted the resistivity data at 50 K against  $\langle r_A \rangle$  in Fig. 2.26c. There is a noticeable increase in the resistivity with decreasing  $\langle r_A \rangle$ , with a change in slope around  $1.18$  Å. It is to be noted that below this value of the A-site cation radius, electronic phase separation and charge ordering occur in the perovskite manganites [10].

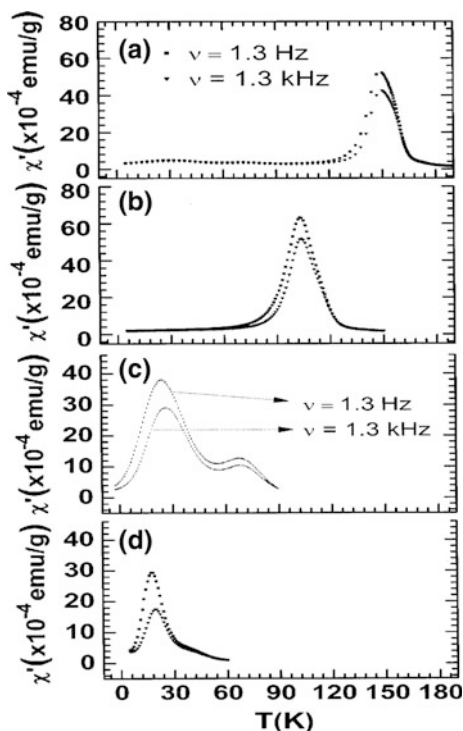
The  $\langle r_A \rangle$  value of  $1.18$  Å in the cobaltates corresponds to  $x \approx 0.6$ ,  $0.49$ ,  $0.24$ , and  $0.195$ , respectively, in the Pr, Nd, Gd, and Dy substituted series of perovskite cobaltites and denoted these compositions as  $x_c$  [23]. It appears that the small magnetic cluster regime becomes prominent around  $x_c$  or  $\langle r_A^c \rangle$ . The low-temperature



peak in the AC susceptibility data is frequency dependent; the small magnetic cluster regime at small  $\langle r_A \rangle$  in the  $\text{La}_{0.7-x}\text{Ln}_x\text{Ca}_{0.3}\text{CoO}_3$  system is considered as the regime to be magnetically inhomogeneous. The inhomogeneous nature of the perovskite cobaltites prevails over the entire range of compositions ( $x = 0.0\text{--}0.7$ ). Hence, with a composition close to  $x_c$  or  $\langle r_A \rangle$ , there is a marked change in the distribution of the magnetic species. Thus, when  $x < x_c$  or  $\langle r_A \rangle > \langle r_A^c \rangle$ , relatively large ferromagnetic clusters or domains are present in the system, resulting in large magnetization and  $T_C$  values. When  $x > x_c$  or  $\langle r_A \rangle < \langle r_A^c \rangle$ , the magnetic clusters become small in size. The ferromagnetic clusters being hole-rich, the electrical resistivity data show changes around the same compositions as the magnetization data, the compositions with  $\langle r_A \rangle > \langle r_A^c \rangle$  exhibiting lower resistivities and near-zero temperature coefficients of resistivity. Owing to the change in the nature of magnetic species around  $x_c$  or  $\langle r_A \rangle$  as a mere change in size distribution, we designated this as a case of phase separation since more than one transition is observed in the AC susceptibility data. The phase-separated regime here involves the coexistence of large ferromagnetic clusters, which are hole-rich and small clusters which are hole-poor [23].

Accordingly, AC susceptibility (Fig. 2.28a) of perovskite  $\text{La}_{0.7}\text{Ca}_{0.3}\text{CoO}_3$  ( $x = 0.0$ ,  $\langle r_A \rangle = 1.354 \text{ \AA}$ ) shows frequency-independent transition around 150 K corresponding to the FM transition, while  $\text{Pr}_{0.7}\text{Ca}_{0.3}\text{CoO}_3$  ( $x = 0.7$ ,  $\langle r_A \rangle = 1.179 \text{ \AA}$ )

**Fig. 2.28** Temperature variation of the AC susceptibility of  
**a**  $\text{La}_{0.7}\text{Ca}_{0.3}\text{CoO}_3$ ,  
**b**  $\text{La}_{0.4}\text{Pr}_{0.3}\text{Ca}_{0.3}\text{CoO}_3$ ,  
**c**  $\text{Pr}_{0.7}\text{Ca}_{0.3}\text{CoO}_3$ , and  
**d**  $\text{Nd}_{0.7}\text{Ca}_{0.3}\text{CoO}_3$  at two different frequencies (adapted from Ref. [23])



shows two distinct transitions, the low temperature one with a greater frequency dependence (Fig. 2.28c). Perovskite cobaltite  $\text{La}_{0.4}\text{Pr}_{0.3}\text{Ca}_{0.3}\text{CoO}_3$  ( $\langle r_A \rangle = 1.194 \text{ \AA}$ ) also shows a single transition corresponding to the  $T_C$  which is frequency independent similar to  $\text{La}_{0.7}\text{Ca}_{0.3}\text{CoO}_3$ . The frequency-independent high-temperature transition in perovskite  $\text{Pr}_{0.7}\text{Ca}_{0.3}\text{CoO}_3$  is due to the large magnetic clusters (akin to cluster glass [25]) as in  $x = 0.0$  composition and the low-temperature transition is due to small magnetic clusters which seem to show some spin glass characteristics. Thus, with the increase in  $x$  or decrease in  $\langle r_A \rangle$  for the  $\text{La}_{0.7-x}\text{Ln}_x\text{Ca}_{0.3}\text{CoO}_3$ , the large ferromagnetic clusters seem to progressively give way to the small clusters, giving rise to magnetic phase separation.

The presence of very weak features at low temperatures in the AC susceptibility data of  $\text{La}_{0.7}\text{Ca}_{0.3}\text{CoO}_3$  indicates that the proportion of small clusters is negligible. Whereas for  $\text{Nd}_{0.7}\text{Ca}_{0.3}\text{CoO}_3$  a frequency-dependent low-temperature transition (around 20 K) due to the small magnetic clusters (Fig. 2.28d). It is instructive to discuss the nature of the spin states of cobalt in  $\text{La}_{0.7-x}\text{Ln}_x\text{Ca}_{0.3}\text{CoO}_3$  series. The magnetic moment of the cobalt ion provides an average magnetic moment value of  $4.5 \mu_B$  per cobalt ion in all the series of perovskite cobaltites. This value suggests that the cobalt ions are in the intermediate-spin (IS) and/or high-spin (HS) states. The IS and HS states of  $\text{Co}^{3+}$  correspond to the electronic configurations  $t_{2g}^5 e_g^1$  ( $S = 1$ ) and  $t_{2g}^4 e_g^2$  ( $S = 2$ ), respectively, and those of  $\text{Co}^{4+}$  to  $t_{2g}^4 e_g^1$  ( $S = 3/2$ ) and  $t_{2g}^3 e_g^2$  ( $S = 5/2$ ). The spin state transitions in the perovskite cobaltites have shown that at high temperatures, the cobalt ions are mostly in the IS or the HS state ref. At low temperatures, some of the cobalt ions may go to the low-spin (LS) state, corresponding to the  $t_{2g}^6$  ( $S = 0$ ) and  $t_{2g}^5$  ( $S = 1/2$ ) configurations in  $\text{Co}^{3+}$  and  $\text{Co}^{4+}$  ions, respectively. The ferromagnetic clusters present prominently at  $x < x_c$  or  $\langle r_A \rangle > \langle r_A^c \rangle$  involve cobalt ions in the IS or HS states. The ferromagnetic regime will therefore be hole-rich, the size of the clusters or the domains decreasing with increasing  $x$  or decreasing  $\langle r_A \rangle$  [23].

The magnetic and electrical properties of polycrystalline  $\text{La}_{0.7-x}\text{Ln}_x\text{Ca}_{0.3}\text{CoO}_3$  ( $\text{Ln} = \text{Pr}, \text{Nd}, \text{Gd}, \text{and Dy}$ ) series are understood in terms of a phase separation scenario wherein large carrier-rich ferromagnetic clusters and carrier-poor smaller clusters coexist at some compositions. The ferromagnetic clusters prominent at small  $x$  are hole-rich, and a change in the electrical resistivity behavior is observed at a critical value  $x_c$ , where the size distribution of magnetic clusters undergoes significant changes. The critical value of  $x$  in the four series of perovskite cobaltites corresponds to the critical value of radius,  $\langle r_A^c \rangle$ , of  $1.18 \text{ \AA}$ , a value where rare earth manganites of the type  $\text{La}_{0.7-x}\text{Ln}_x\text{Ca}_{0.3}\text{MnO}_3$  ( $\text{Ln} = \text{Nd}, \text{Gd}, \text{and Y}$ ) are known to exhibit charge ordering and EPS prominently [10]. It appears that around  $\langle r_A^c \rangle$  or  $x_c$ , a significant change occurs in the e.g. bandwidth and the charge carriers become more localized, causing changes in the magnetic and electron transport properties. It is well to recall that the electrical resistivity and ferromagnetism in the perovskite cobaltites are linked to the presence of the  $\text{Co}^{3+}\text{--O--Co}^{4+}$  species with the appropriate spin states of cobalt ions. The magnetism in the perovskite cobaltites is due to  $\text{Co}^{3+}\text{--O--Co}^{4+}$  superexchange, but most of the  $\text{Ln}_{1-x}\text{A}_x\text{CoO}_3$  also seems to show evidence for some frustration at low temperature, as though there is no long-range

ferromagnetism. In order to understand the nature of these materials, we have further discussed the magnetic properties of  $\text{Ln}_{0.7}\text{Ca}_{0.3}\text{CoO}_3$  and  $\text{La}_{1-x}\text{Sr}_x\text{CoO}_3$  cobaltites, down to low temperatures.

### 2.3.2 Spin Glass Behavior in $\text{Ln}_{0.7}\text{Ca}_{0.3}\text{CoO}_3$ ( $\text{Ln} = \text{La}, \text{Pr}, \text{and Nd}$ )

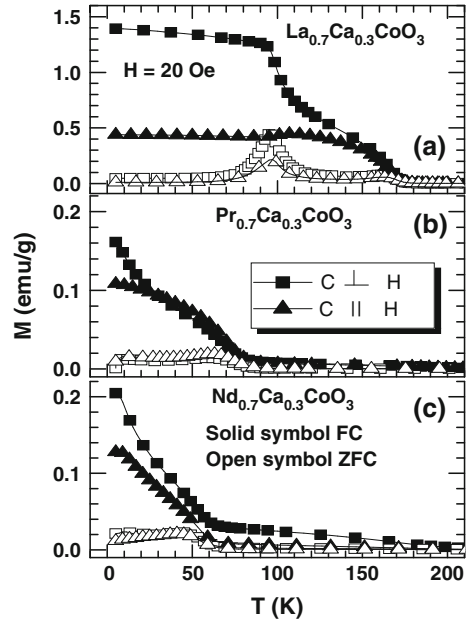
Preliminary DC magnetic susceptibilities of polycrystalline as well single crystalline samples of  $\text{Ln}_{0.7}\text{Ca}_{0.3}\text{CoO}_3$  series ( $\text{Ln} = \text{La}, \text{Pr}, \text{and Nd}$ ) showed that while  $\text{La}_{0.7}\text{Ca}_{0.3}\text{CoO}_3$  clearly exhibits a ferromagnetic-type transition ( $T_C \sim 175$  K),  $\text{Pr}_{0.7}\text{Ca}_{0.3}\text{CoO}_3$  and  $\text{Nd}_{0.7}\text{Ca}_{0.3}\text{CoO}_3$  do not show distinct ferromagnetic transitions. There is a slight increase in the magnetization of  $\text{Pr}_{0.7}\text{Ca}_{0.3}\text{CoO}_3$  around 75 K, but not due to a long-range ferromagnetic transition. The magnetic behavior of a single crystal of  $\text{Pr}_{0.7}\text{Ca}_{0.3}\text{CoO}_3$  is similar to that of the polycrystalline sample [23]. The large drop in the magnetic moment at low temperatures in the Pr and Nd derivatives is noteworthy. In order to understand the nature of these materials, we have discussed the magnetic properties of  $\text{Ln}_{0.7}\text{Ca}_{0.3}\text{CoO}_3$  in detail, down to low temperatures. The electronic phase separation and associated magnetic properties of  $\text{Pr}_{0.7}\text{Ca}_{0.3}\text{CoO}_3$  and  $\text{Nd}_{0.7}\text{Ca}_{0.3}\text{CoO}_3$  arise because of the small average size of the A-site cations. In these perovskite cobaltites, the average radius (for orthorhombic structure) is less than 1.18 Å, which is the critical value only above which long-range ferromagnetism manifests [23]. It is known that increase in size disorder and decrease in size of the A-site cations favor EPS.

Figure 2.29 shows temperature dependence of the ZFC and FC magnetization of single crystalline perovskites  $\text{Ln}_{0.7}\text{Ca}_{0.3}\text{CoO}_3$  ( $\text{Ln} = \text{La}, \text{Pr}, \text{or Nd}$ ) measured parallel and perpendicular to the c-axis in an applied field of 20 Oe.

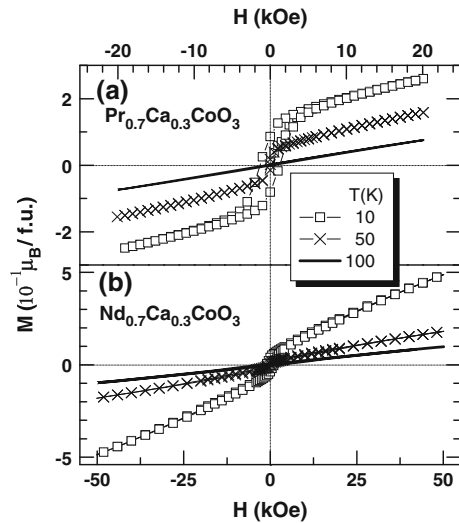
Perovskite  $\text{La}_{0.7}\text{Ca}_{0.3}\text{CoO}_3$  shows a distinct FM-type transition in the FC data around 170 K ( $T_C$ ), while the ZFC data show a cluster glass transition around 95 K. Whereas,  $\text{Pr}_{0.7}\text{Ca}_{0.3}\text{CoO}_3$  and  $\text{Nd}_{0.7}\text{Ca}_{0.3}\text{CoO}_3$  cobaltites do not, however, show such a ferromagnet-type behavior. The irreversible temperature,  $T_{\text{irr}}$ , between the ZFC and FC in perovskites  $\text{Pr}_{0.7}\text{Ca}_{0.3}\text{CoO}_3$  and  $\text{Nd}_{0.7}\text{Ca}_{0.3}\text{CoO}_3$  persists up to 200 K unlike in the  $\text{La}_{0.7}\text{Ca}_{0.3}\text{CoO}_3$ . The  $T_{\text{irr}}$ , however, decreases with the increasing magnetic field. The inverse susceptibility data could be fitted to Curie–Weiss behavior with the extrapolated Weiss temperatures,  $\theta_p$ , of 150 K, –180 K, and –340 K for the La, Pr, and Nd derivatives, respectively. The negative  $\theta_p$  values in the latter cobaltites imply the presence of antiferromagnetic interactions in the high-temperature region, while for La derivative the interaction is FM.

The  $M(H)$  loops for  $\text{Pr}_{0.7}\text{Ca}_{0.3}\text{CoO}_3$  and  $\text{Nd}_{0.7}\text{Ca}_{0.3}\text{CoO}_3$  perovskites at different temperatures are presented in Fig. 2.30. These perovskite cobaltites show hysteresis loops at low temperatures ( $\leq 10$  K) and a nonsaturating behavior up to 5 Tesla. The coercive field and remanent magnetization are almost the same in both the orientations for all three cobaltites.

**Fig. 2.29** Temperature dependence of the ZFC and FC magnetization,  $M$ , of  $\text{Ln}_{0.7}\text{Ca}_{0.3}\text{CoO}_3$  where **a**  $\text{Ln} = \text{La}$ , **b**  $\text{Ln} = \text{Pr}$ , and **c**  $\text{Ln} = \text{Nd}$ , at  $H = 20$  Oe measured parallel (*triangle*) and perpendicular (*square*) to the  $c$ -axis (adapted from Ref. [23])

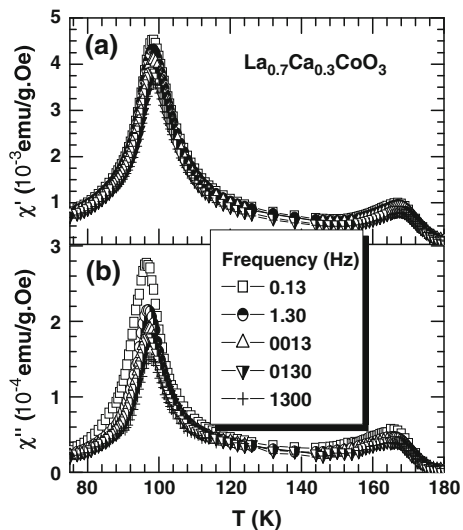


**Fig. 2.30** The hysteresis curves for **a**  $\text{Pr}_{0.7}\text{Ca}_{0.3}\text{CoO}_3$  **b**  $\text{Nd}_{0.7}\text{Ca}_{0.3}\text{CoO}_3$  at different temperatures measured parallel to the  $c$ -axis (adapted from Ref. [23])



The magnetic behaviors of  $\text{Ln}_{0.7}\text{Ca}_{0.3}\text{CoO}_{-3}$  perovskites have been discussed in terms of AC susceptibility and magnetic relaxation measurements which are useful to investigate the magnetic glassy behavior [23]. Figure 2.31 shows the AC susceptibility of  $\text{La}_{0.7}\text{Ca}_{0.3}\text{CoO}_3$  below Curie temperature ( $T_C$ ), which is in accordance with the low field ZFC magnetization. Two distinct peaks: a frequency-independent high-temperature peak (170 K) that indicates a ferromagnetic ordering and a low

**Fig. 2.31** The temperature dependence of the **a** In-phase and **b** Out-of-phase AC susceptibility of  $\text{La}_{0.7}\text{Ca}_{0.3}\text{CoO}_3$  at different frequencies (adapted from Ref. [23])



temperature frequency-dependent peak at 100 K. The AC susceptibility for  $\text{Pr}_{0.7}\text{Ca}_{0.3}\text{CoO}_3$  and  $\text{Nd}_{0.7}\text{Ca}_{0.3}\text{CoO}_3$  exhibits a frequency-dependent maximum around 70 K for  $\text{Pr}_{0.7}\text{Ca}_{0.3}\text{CoO}_3$  (Fig. 2.32). With increasing frequency, the peak value shifts toward higher temperatures.  $\text{Nd}_{0.7}\text{Ca}_{0.3}\text{CoO}_3$  shows a peak around 55 K as shown in Fig. 2.32. Thus, with decrease in the average radius of the A-site cations,  $\langle r_A \rangle$ , the magnetic transition temperature as revealed by the AC susceptibility maximum shifts to lower temperatures.

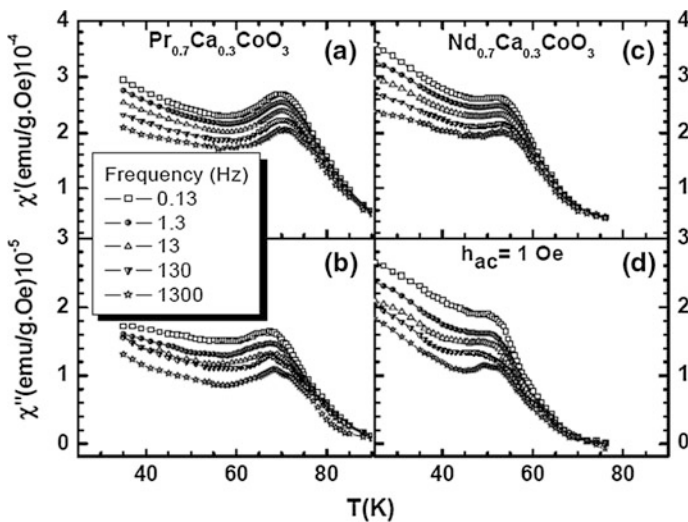
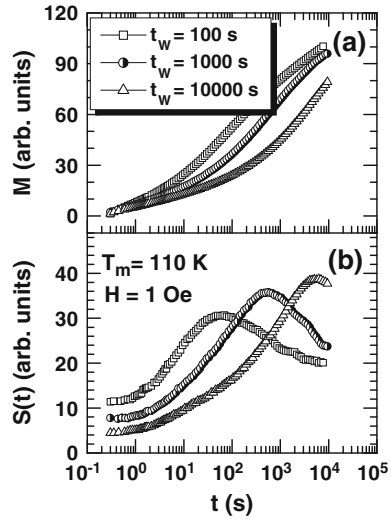


**Fig. 2.32** Temperature dependence magnetic AC susceptibility for **a, b**  $\text{Pr}_{0.7}\text{Ca}_{0.3}\text{CoO}_3$  and **c, d**  $\text{Nd}_{0.7}\text{Ca}_{0.3}\text{CoO}_3$  at different frequencies (adapted from Ref. [23])

**Fig. 2.33** ZFC-relaxation measurements on  $\text{La}_{0.7}\text{Ca}_{0.3}\text{CoO}_3$  at  $T_m = 110$  K for different waiting times (adapted from Ref. [23])



The ZFC time-dependent magnetic relaxation for  $\text{La}_{0.7}\text{Ca}_{0.3}\text{CoO}_3$  is a consequence of nonequilibrium spin-glass-like state (Fig. 2.33). The long-time relaxations of the magnetization and aging phenomena well known in spin glasses [21] are commonly found in many other random magnetic systems. In Fig. 2.33 an aging behavior, similar to spin glasses revealed by an inflection point in the magnetization versus  $\log(t)$  plot and a corresponding maximum in the relaxation rate curves at an observation time close to the wait time. The aging-dominated relaxation is strikingly similar to the behavior of conventional spin glasses. In the latter situation, aging is interpreted within the droplet model (or domain growth) for spin glasses to reflect the growth of equilibrium spin glass domains, with the maximum in the relaxation rate being associated with a crossover between quasi-equilibrium (from processes within ordered spin glass domains) and nonequilibrium dynamics (processes governed by effects at domain walls) [21].

Similarly, the time-dependent ZFC magnetization for  $\text{Pr}_{0.7}\text{Ca}_{0.3}\text{CoO}_3$  and  $\text{Nd}_{0.7}\text{Ca}_{0.3}\text{CoO}_3$  exhibits logarithmical dynamics below the transition temperature (70 and 55 K). The relaxation rate attains a maximum at the elapsed time, close to the wait time, indicating a pronounced age-dependent effect. Such a behavior is generally observed in spin glasses and explained within the droplet (or domain growth) model [21].

A key property to understand and model the dynamics of spin glasses is the occurrence of memory. A characteristic of the spin glass phase (ordinary or reentrant) is the memory behavior, whereas a disordered and frustrated ferromagnetic phase would show little or no memory effect. Figure 2.34a shows a memory dip for  $\text{La}_{0.7}\text{Ca}_{0.3}\text{CoO}_3$  (at 85 K), indicating the spin-glass-type phase. At 110 K, on the other hand, a memory dip can barely be discerned, signifies that the system is confined in a disordered ferromagnetic phase.

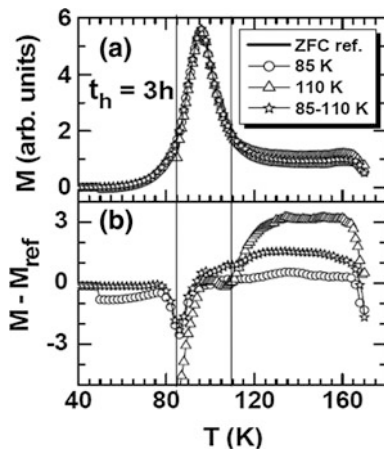
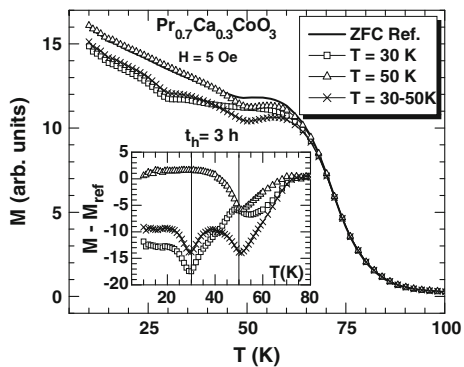


**Fig. 2.34** The ZFC magnetization memory experiment on  $\text{La}_{0.7}\text{Ca}_{0.3}\text{CoO}_3$ ; **a** the temperature dependence of ZFC magnetization,  $M$ , (reference curve) and memories of two temperature stops (at 85 and 110 K) during cooling each for 3 h and **b** the difference ( $M - M_{\text{ref}}$ ) plot of the respective curves (adapted from Ref. [23])

**Fig. 2.35** The ZFC magnetization memory experiment on  $\text{Pr}_{0.7}\text{Ca}_{0.3}\text{CoO}_3$  (adapted from Ref. [23])

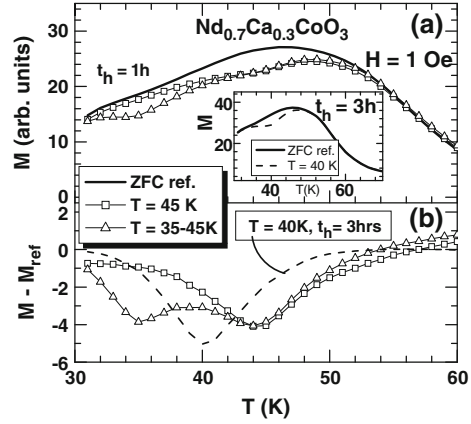


Likewise, a memory effect is observed for  $\text{Pr}_{0.7}\text{Ca}_{0.3}\text{CoO}_3$  (Fig. 2.35) and  $\text{Nd}_{0.7}\text{Ca}_{0.3}\text{CoO}_3$  at different temperatures (Fig. 2.36). The memory dips are more prominent at low temperature for both the perovskites and correlate the spin-glass-like phases at the low temperatures [23].

### 2.3.3 Spin Glass Behavior in $\text{La}_{1-x}\text{Sr}_x\text{CoO}_3$

The hole-doped perovskite cobaltite  $\text{La}_{1-x}\text{Sr}_x\text{CoO}_3$  is a model system to discuss the EPS and spin glass phenomenon because of the absence of charge ordering, FM insulating, and the long-range AFM ordering, which make it easier to probe and

**Fig. 2.36** The ZFC magnetization memory experiment on  $\text{Nd}_{0.7}\text{Ca}_{0.3}\text{CoO}_3$  (adapted from Ref. [23])



understand the spin glass phenomenon [26–28]. Substituting divalent  $\text{Sr}^{2+}$  ions at trivalent  $\text{La}^{3+}$  sites in  $\text{LaCoO}_3$  causes spontaneous nanoscopic phase separation where nanosized (i.e., 1–3 nm) hole-rich FM metallic clusters are embedded in a hole-poor insulating non-FM matrix [28]. The interaction between  $\text{Co}^{4+}$  and  $\text{Co}^{3+}$  is FM double exchange, whereas the  $\text{Co}^{3+}$ - $\text{Co}^{3+}$  and  $\text{Co}^{4+}$ - $\text{Co}^{4+}$  are antiferromagnetic [27, 28]. For low doping, these two competitive interactions are random and frustrated, which leads to the glassy magnetic behavior for the doping range  $0.0 < x < 0.18$  as shown in the magnetic phase diagram of Fig. 2.37 [27, 28]. With increasing doping level, the number and size of the hole-rich FM clusters increase rapidly, and the percolation of these FM clusters at a critical doping value,  $x_p$  of 0.18, yields a crossover from short-range to long-range FM ordering [28]. Accumulated experimental data from various high-resolution probes reveal that the EPS in  $\text{La}_{1-x}\text{Sr}_x\text{CoO}_3$  cobaltite is confined to a well-defined doping range,

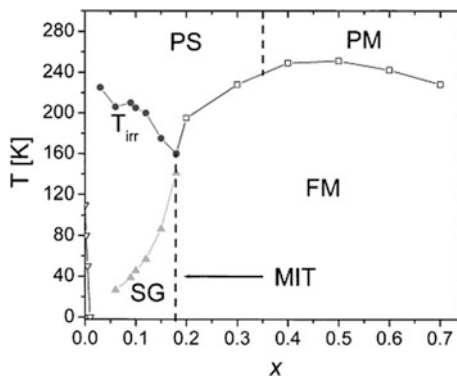
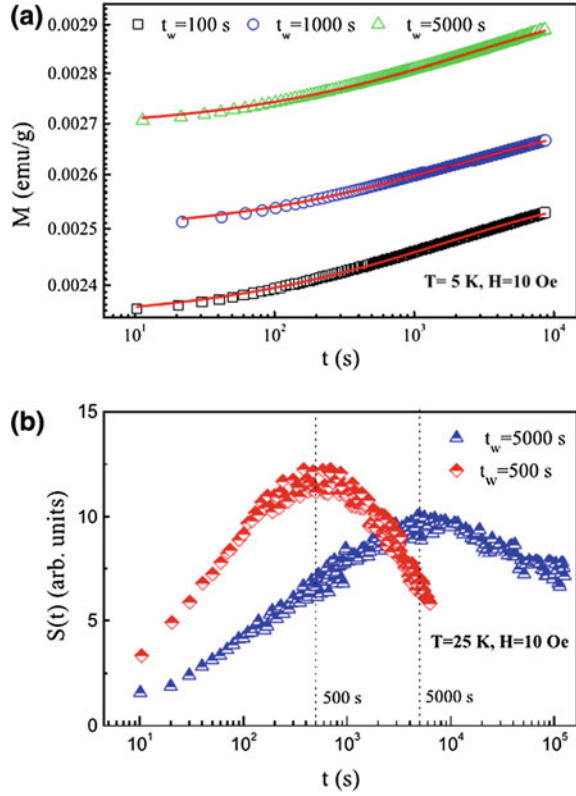


**Fig. 2.37** Magnetic phase diagram for  $\text{La}_{1-x}\text{Sr}_x\text{CoO}_3$ . *PS* paramagnetic semiconductor, *PM* paramagnetic metal, *FM* ferromagnetic metal, *SG* spin glass, *MIT* metal-insulator transition, and  $T_{\text{irr}}$  is the irreversibility temperature which marks the bifurcation of ZFC and FC dc magnetization curves (adapted from Ref. [28])



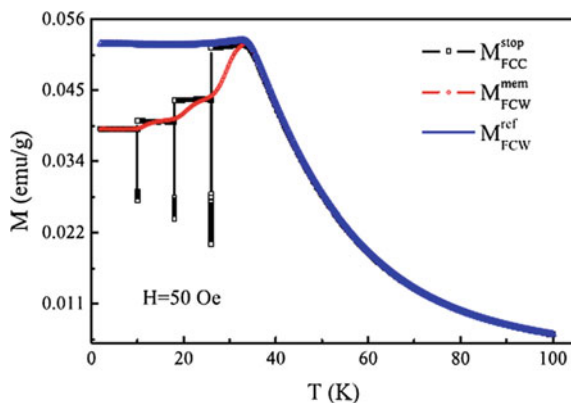
**Fig. 2.38** ZFC-relaxation measurements on  $\text{La}_{0.9}\text{Sr}_{0.1}\text{CoO}_3$  (adapted from Ref. [29])



$0.04 < x < 0.22$ , which covers both the FM and glassy magnetic states (Fig. 2.37). It is fascinating to explore whether the phase-separated states in  $\text{La}_{1-x}\text{Sr}_x\text{CoO}_3$  cobaltites exhibiting glassy magnetic behavior resemble that of a canonical/atomic spin glass or a superparamagnetic system or an assembly of strongly interacting magnetic clusters. Wu et al. [28] have pointed out that at lower Sr doping ( $x < 0.18$ ) the system enters a mixed phase that displays the characteristics of both a spin glass and a ferromagnet. A cusp in the zero-field-cooled DC magnetization, a frequency-dependent peak in the AC susceptibility and time-dependent effects in both DC and AC magnetic properties all point toward glassy behavior. However, for high Sr doping ( $x > 0.2$ ) the system exhibits unconventional ferromagnetism with a Curie temperature up to 250 K, which is interpreted in terms of the coalescence of short-range-ordered FM clusters.

Earlier studies on polycrystalline  $\text{La}_{1-x}\text{Sr}_x\text{CoO}_3$  ( $0 < x < 0.15$ ) cobaltites showed (Fig. 2.37) the presence of multiple glassy magnetic phases at low temperatures and also are superparamagnetic below the irreversibility temperature  $T_{\text{irr}}$  [27, 28]. Recent, investigations by Khan et al. [29], in single crystalline  $\text{La}_{0.9}\text{Sr}_{0.1}\text{CoO}_3$  cobaltite of magnetic relaxation and memory effects below the freezing temperature  $T_f$ , reveal the characteristics of the spin glass phase. The magnetic relaxation is

**Fig. 2.39** The ZFC magnetization memory experiment on  $\text{La}_{0.9}\text{Sr}_{0.1}\text{CoO}_3$  (adapted from Ref. [29])



described well by the stretched exponential function and shows that the system evolves through a number of intermediate states.

The analysis of the magnetic relaxation rate at different temperatures and magnetic fields shows (Fig. 2.38) that the glassy behavior of single-crystalline  $\text{La}_{0.9}\text{Sr}_{0.1}\text{CoO}_3$  cobaltite resembles that of a true spin glass phase akin to single-crystalline  $\text{Ln}_{0.7}\text{Ca}_{0.3}\text{CoO}_3$  cobaltites [23], where only the intercluster interaction is the origin of the glassy behavior. The observed spin glass behavior in the single-crystalline  $\text{La}_{0.9}\text{Sr}_{0.1}\text{CoO}_3$  cobaltite is believed to be due to the random distribution of FM and AFM interactions in the perovskite [29].

Memory effects presented in Fig. 2.39 at different temperature and field-cycling experiments, show that the single-crystalline  $\text{La}_{0.9}\text{Sr}_{0.1}\text{CoO}_3$  cobaltite is capable of retaining the magnetization history even for a large change in the magnetization. The presence of memory dips in the ZFC magnetization suggests that glassy magnetic behavior in single-crystalline  $\text{La}_{0.9}\text{Sr}_{0.1}\text{CoO}_3$  cobaltite originates from spin–spin interaction, unlike the independent relaxation of clusters, which gives rise to superparamagnetic behavior. The effects of positive and negative temperature changes on the reversion of the original spin configuration suggest that the memory phenomena in this perovskite cobaltite follow the hierarchical model of spin glass [21, 22].

## References

1. E.O. Wollan, W.C. Koehler, Phys. Rev. **100**, 545 (1955); W.C. Koehler, E.O. Wollan, J. Phys. Chem. Solids **2**, 100, (1957); C.N.R. Rao, A.K. Cheetham, R. Mahesh, Chem. Mater. **8**, 2421 (1996); E.L. Nagaev, Phys. Usp **39**, 781 (1996); C.N.R. Rao, Chem. Eur. J. **2**, 1499 (1996); A. P. Ramirez, J. Phys.: Condens. Matter **9**, 8171 (1997); C.N.R. Rao, B. Raveau (eds.), *Colossal Magnetoresistance, Charge-Ordering and Related Properties of Manganese Oxides* (World Scientific, Singapore, 1998); A. Mareo, S. Yunoki, E. Dagotto, Science **283**, 2034 (1999); C. N.R. Rao, A. Arulraj, A.K. Cheetham, B. Raveau, J. Phys.: Condens. Matter **12**, R83 (2000); Y. Tokura, *Colossal Magnetoresistive Oxides* (Gordon and Breach, NewYork, 2000)

2. E. Dagotto, T. Hotta, A. Moreo, *Phys. Rep.* **344**, 1 (2001); E. Dagotto, *Nanoscale Phase Separation and Colossal Magnetoresistance: The Physics of Manganites and Related Compounds* (Springer, Berlin, New York, 2003); N.D. Mathur et al., *Phys. Today* **56**, 25, (2003); C.N.R. Rao, A.K. Kundu, M.M. Seikh, L. Sudheendra, *Dalton Trans.* **19**, 3003 (2004); V.B. Shenoy et al., *Phys. Rev. Lett.*, **98**, 097201 (2007); V.B. Shenoy, C.N.R. Rao, *Phil. Trans. R. Soc. A* **366**, 63 (2008); V.B. Shenoy et al., *Chem. Phys. Chem.* **7**, 2053, (2010); B. Raveau, M.M. Seikh, *Cobalt Oxides: From Crystal Chemistry to Physics* (Wiley-VCH, 2012)
3. L.M. Rodriguez-Martinez, J.P. Attfield, *Phys. Rev. B* **54**, R15622 (1996); J.P. Attfield, *Chem. Mater.* **10**, 3239 (1998)
4. J.M.D. Teresa, M.R. Ibarra, P.A. Algarabel, C. Ritter, C. Marquina, J. Blasco, J. Garcia, A.D. Moral, Z. Arnold, *Nature* **386**, 256, (1997); D.E. Cox, P.G. Radealli, M. Marezio, S-W. Cheong, *Phys. Rev. B* **57**, 3305 (1998); S. Marcone et al., *Phys. Rev. B* **68**, 094422 (2003)
5. P.G. Radealli, R.M. Ibberson, D.N. Argyriou, H. Casalta, K.H. Andersen, S.-W. Cheong, J.F. Mitchell, *Phys. Rev. B* **63**, 172419 (2001)
6. G.S. Bhalla, S. Selcuk, T. Dhakal, A. Biswas, A.F. Hebard, *Phys. Rev. Lett.* **102**, 077205 (2009); Y. Murakami et al., *Nat. Nanotech.* **5**, 37 (2010); T.Z. Ward, Z. Gai, H.W. Guo, L.F. Yin, J. Shen, *Phys. Rev. B* **83**, 125125 (2011); D. Niebieskikwiat, R.D. Sánchez, *J. Phys.: Condens. Mater.* **24**, 436001 (2012)
7. A. Moreo, S. Yunoki, E. Dagotto, *Science* **283**, 2034 (1999); M. Fäth et al., *Science* **285**, 1540, (1999); M.R. Freeman et al. *Science* **294**, 1484, (2001); J. C. Loudon et al., *Nature* **420**, 797, (2002); Ch. Renner, G. Aeppli, B.G. Kim, Y.A. Soh, S.W. Cheong, *Nature* **416**, 518 (2002); L. Zhang et al., *Science* **298**, 805, (2002); L. Ghivelder, F. Parisi, *Phys. Rev. B* **71**, 184425 (2005); E. Dagotto, *Science*, **309**, 257 (2005); V. B. Shenoy et al., *Phys. Rev. Lett.* **98**, 097201 (2007); J. Tao et al., *Phys. Rev. Lett.* **103**, 097202 (2009); Liang et al., *Nanoscale Res. Lett.* **9**, 325 (2014) and references therein
8. C.N.R. Rao, A.R. Raju, V. Ponnambalam, S. Parashar, N. Kumar, *Phys. Rev. B* **61**, 594 (2000); S. Srivastava, N.K. Pandey, P. Padhan, R.C. Budhani, *Phys. Rev. B* **62**, 13868 (2001); R.C. Budhani, N.K. Pandey, P. Padhan, S. Srivastava, R.P.S. M. Lobo, *Phys. Rev. B* **65**, 14429 (2002)
9. M. Uehara, S. Mori, C.H. Chen, S-W. Cheong, *Nature (London)* **399**, 560 (1999); P.B. Littlewood, *Nature (London)* **399**, 529 (1999). V. Podzorov, M. Uehara, M.E. Gershenson, T. Y. Koo, S.W. Cheong, *Phys. Rev. B* **61**, R3784 (2000)
10. L. Sudheendra, C.N.R. Rao, *J. Phys.: Condens. Mater.* **15**, 3029 (2003); A.K. Kundu, P.V. Vanitha, C.N.R. Rao, *Solid State Comm.* **125**, 41 (2003)
11. A.M. Balagurov, VYu. Pomjakushin, D.V. Sheptyakov, V.L. Aksenov, P. Fischer, L. Keller, OYu. Gorbenco, A.R. Kaul, N.A. Babushkina, *Phys. Rev. B* **64**, 24420 (2001)
12. H. Terashita, J.J. Neumeier, *Phys. Rev. B* **63**, 174436 (2001)
13. J.M. de Teresa, M.R. Ibarra, J. Garcia, J. Blasco, C. Ritter, P.A. Algarabel, C. Marquina, A. del Moral, *Phys. Rev. Lett.* **76**, 3392 (1996)
14. I.G. Deac, S.V. Diaz, B.G. Kim, S.-W. Cheong, P. Schiffer, *Phys. Rev. B* **65**, 174426 (2002)
15. A.K. Kundu, M.M. Seikh, K. Ramesha, C.N.R. Rao, *J. Phys.: Condens. Mater.* **17**, 4171 (2005); A.K. Kundu, P. Nordblad, C.N.R. Rao, *J. Phys.: Condens. Mater.* **18**, 4809 (2006)
16. A. Maignan, C. Martin, M. Hervieu, B. Raveau, J. Hejtmanek, *Solid State Commun.* **107**, 363 (1998); I.O. Troyanchuk, D.D. Khalyavin, S.V. Trukhanov, H. Szymczak, *J. Phys.: Condens. Matter* **11**, 8707 (1999)
17. P.M. Woodward, D.E. Cox, T. Vogt, C.N.R. Rao, A.K. Cheetham, *Chem. Mater.* **11**, 3528 (1999)
18. C. Ritter, R. Mahendiran, M.R. Ibarra, L. Morellon, A. Maignan, B. Raveau, C.N.R. Rao, *Phys. Rev. B* **61**, R9229 (2000)
19. P.V. Vanitha, C.N.R. Rao, *J. Phys.: Condens. Mater.* **13**, 11707 (2001)
20. H. Kuwahara, Y. Tomioka, A. Asamitsu, Y. Moritomo, Y. Tokura, *Science* **270**, 961 (1995); P.V. Vanitha, R.S. Singh, S. Natarajan, C.N.R. Rao, *J. Solid. State. Chem.* **137**, 365 (1998); P.V. Vanitha, A. Arulraj, A.R. Raju, C.N.R. Rao, *C.R. Acad. Sci. Paris*, **2**, 595 (1999)

21. J.A. Mydosh, in *Spin Glasses: An Experimental Introduction* (Taylor and Francis, London, 1993); K. Binder, A.P. Young, *Rev. Mod. Phys.* **58**, 801 (1986)
22. D.N.H. Nam, R. Mathieu, P. Nordblad, N.V. Khiem, N.X. Phuc, *Phys. Rev. B* **62**, 1027 (2000)
23. A.K. Kundu, K. Ramesha, R. Seshadri, C.N.R. Rao, *J. Phys.: Condens. Mater.* **16**, 7955 (2004); A.K. Kundu, P. Nordblad, C.N.R. Rao, *Phys. Rev. B* **72**, 144423 (2005); A.K. Kundu, P. Nordblad, C.N.R. Rao, *J. Solid State Chem.* **179**, 923 (2006)
24. C. He, S. El-Khatib, J. Wu, J.W. Lynn, H. Zheng, J.F. Mitchell, C. Leighton, *Euro. Phys. Lett.*, **87**, 27006 (2009); F. Guillou, Q. Zhang, Z. Hu, C.Y. Kuo, Y.Y. Chin, H.J. Lin, C.T. Chen, A. Tanaka, L.H. Tjeng, V. Hardy, *Phys. Rev. B* **87**, 115114 (2013); D. Phelan, K.P. Bhatti, M. Taylor, S. Wang, C. Leighton, *Phys. Rev. B* **89**, 184427 (2014) and references therein
25. M. Itoh, I. Natori, S. Kubota, K. Matoya, *J. Phys. Soc. Jpn.* **63**, 1486 (1994)
26. J. Wu, J.W. Lynn, C.J. Glinka, J. Burley, H. Zheng, J.F. Mitchell, C. Leighton, *Phys. Rev. Lett.* **94**, 037201 (2005); D. Fuchs et al., *Phys. Rev. B* **71**, 92406 (2005); M.W. Haverkort et al., *Phys. Rev. Lett.* **97**, 176405 (2006); A.K. Kundu et al., *J. Solid State Chem.* **180**, 1318, (2007); J. Yu et al., *Phys. Rev. B* **80**, 052402, (2009); C. He et al., *Phys. Rev. B* **80**, 214411, (2009)
27. P.M. Raccach et al., *Phys. Rev.* **155**, 932 (1967); V.G. Bhide, D.S. Rajoria, C.N.R. Rao, G.R. Rao, V.G. Jadhao, *Phys. Rev. B* **12**, 2832 (1975); M.A. Senaris Rodriguez et al., *J. Solid State Chem.* **118**, 323 (1995); V. G. Sathe et al., *J. Phys.: Condens. Mater.* **8**, 3889 (1996); M. Imada et al., *Rev. Mod. Phys.* **70**, 1039, (1998); R. Caciuffo et al., *Phys. Rev. B* **59**, 1068 (1999); R. Ganguly et al., *J. Phys. Condens. Matter* **13**, 10911, (2001); V.G. Prokhorov et al., *Phys. Rev. B* **66**, 132410 (2002); R. Mahendiran et al., *Phys. Rev. B* **68**, 24427, (2003); L. Sudheendra et al., *Ferroelectrics* **306**, 227 (2004); A. Ghoshray et al., *Phys. Rev. B* **69**, 064424, (2004); M.J.R. Hoch et al., *Phys. Rev. B* **69**, 014425, (2004); S. Tsubouchi et al., *Phys. Rev. B* **69**, 144406, (2004); A.K. Kundu et al., *Solid State Commun.* **134**, 307, (2005); S.R. Giblin et al., *Euro. Phys. Lett.*, **70**, 677 (2005)
28. J. Wu, C. Leighton, *Phys. Rev. B* **67**, 174408 (2003); P.L. Kuhns, M.J.R. Hoch, W.G. Moulton, A.P. Reyes, J. Wu, C. Leighton, *Phys. Rev. Lett.* **91**, 127202 (2003)
29. N. Khan, P. Mandal, D. Prabhakaran, *Phys. Rev. B* **90**, 024421 (2014)

Magnetic Perovskites

Synthesis, Structure and Physical Properties

Kundu, A.K.

2016, XI, 167 p. 133 illus., Hardcover

ISBN: 978-81-322-2759-5